Autophagy 11:5, 796–811; May 2015; © 2015 Taylor & Francis Group, LLC

Uvrag targeting by *Mir125a* and *Mir351* modulates autophagy associated with *Ewsr1* deficiency

Yunha Kim,[1] Young-Sook Kang,[2] Na-Young Lee,[2] Ki Yoon Kim,[1] Yu Jin Hwang,[1] Hyun-Wook Kim,[3] Im Joo Rhyu,[3] Song Her,[4] Min-Kyung Jung,[1] Sun Kim,[5,6] Chai-Jin Lee,[5] Seyoon Ko,[6] Neil W Kowall,[7,8] Sean Bong Lee,[9] Junghee Lee,[7,8] and Hoon Ryu[1,7,8,*]

[1]Laboratory for Neuronal Gene Regulation and Epigenetics; Center for NeuroMedicine; Korea Institute of Science and Technology; Seoul, Korea; [2]Research Center for Cell Fate Control; College of Pharmacy; Sookmyung Women's University; Seoul, Korea; [3]Department of Anatomy; College of Medicine; Korea University; Seoul, Korea; [4]Bio-Imaging Center; Korea Basic Science Institute; Chuncheon, Korea; [5]Interdisciplinary Program in Bioinformatics and Computational Science & Technology; [6]Department of Computer Science and Engineering, and Bioinformatics Institute; Seoul National University; Seoul, Korea; [7]Veteran's Affairs Boston Healthcare System; Boston, MA USA; [8]Boston University Alzheimer's Disease Center and Department of Neurology; Boston University School of Medicine; Boston, MA, USA; [9]Department of Pathology & Laboratory Medicine; Tulane University School of Medicine; New Orleans, LA USA

Keywords: autophagy, EWSR1, *Mir125a*, *Mir351*, UVRAG

Abbreviations: AGO2, argonaute; RISC, catalytic component 2; *Ant-Mir125a*; *Mir125a*-specific antagomir; *Ant-Mir351*; *Mir351*-specific antagomir; ATG5; autophagy-related 5; ATG12; autophagy-related 12; ATG14; autophagy-related 14; BECN1; Beclin 1; CNT-Ant; control antagomir; CQ; chloroquine; DGCR8; DiGeorge syndrome critical region gene 8; EWS; Ewing's Sarcoma; EWSR1; EWS RNA-binding protein 1/Ewing Sarcoma Break Point Region 1; $Ewsr1^{+/+}$; *Ewsr1* wild type; $ewsr1^{-/-}$; *Ewsr1* homozygous knockout; LAMP; lysosomal-associated membrane protein; MAP1LC3/LC3; microtubule-associated protein 1 light chain 3; MEF; mouse embryonic fibroblast; miRNA; microRNA; Pep.A; pepstatin A; pri-miRNA; primary transcript miRNA; RNA-seq; whole transcriptome sequencing; SQSTM1; sequestosome 1; siRNA; small interfering RNA; UVRAG; UV radiation-resistance associated.

The *EWSR1* (EWS RNA-binding protein 1/Ewing Sarcoma Break Point Region 1) gene encodes a RNA/DNA binding protein that is ubiquitously expressed and involved in various cellular processes. EWSR1 deficiency leads to impairment of development and accelerated senescence but the mechanism is not known. Herein, we found that EWSR1 modulates the *Uvrag* (UV radiation resistance associated) gene at the post-transcription level. Interestingly, EWSR1 deficiency led to the activation of the DROSHA-mediated microprocessor complex and increased the level of *Mir125a* and *Mir351*, which directly target *Uvrag*. Moreover, the *Mir125a*- and *Mir351-mediated reduction of Uvrag* was associated with the inhibition of autophagy that was confirmed in *ewsr1* knockout (KO) MEFs and *ewsr1* KO mice. Taken together, our data indicate that EWSR1 is involved in the post-transcriptional regulation of *Uvrag* via a miRNA-dependent pathway, resulting in the deregulation of autophagy inhibition. The mechanism of *Uvrag* and autophagy regulation by EWSR1 provides new insights into the role of EWSR1 deficiency-related cellular dysfunction.

Introduction

The *EWSR1* gene, formerly known as *EWS (*Ewing's Sarcoma), is a member of the *TET* (*FUS/TLS, EWSR1,* and *TAF15*) family genes. EWSR1 acts as an RNA-binding protein and interacts with various splicing factors such as SF1/ZFM1, YBX1, SNRPC/U1C, and SRSF10.[1] The transcriptional activity of EWSR1 involves interactions with subunits of transcription factor II D, CREBBP (CREB binding protein), and RNA polymerase II complexes.[1] In addition, EWSR1 functions as a transcriptional activator for *POU4F1/BRN3A*,[2] *Foxe3/Hnf3* (forkhead box E3),[3,4] *POU5F1/OCT4* (POU class 5 homeobox 1)[5] and *YBX1* (Y box binding protein 1)[6] in a cell-type and promoter-specific manner. *EWSR1* is fused with various transcription factors, including *ATF1* (activating transcription factor 1),[7] *Fli1* (Friend leukemia integration 1),[8] *WT1* (Wilms tumor 1),[9] and *DDIT3/CHOP/GADD153* (DNA-damage-inducible transcript 3).[10] Following fusion of *EWSR1* with DNA-binding transcription factors, *EWSR1-ATF1*, *Ewsr1-Fli1*, and *EWSR1-WT1* regulate cell transformation, proliferation, and viability.[7-10] Recently, Li et al.[11] demonstrated a cell-autonomous defect of precursor B lymphocyte development and a defect in meiosis resulting in massive apoptosis of spermatocytes in *ewsr1*-deficient mice. In addition, EWSR1 deficiency contributes to cellular senescence

*Correspondence to: Hoon Ryu; Email: hoonryu@bu.edu
Submitted: 09/06/2013; Revised: 03/18/2015; Accepted: 03/25/2015
http://dx.doi.org/10.1080/15548627.2015.1035503

in mouse embryonic fibroblasts (MEFs) and in hematopoietic stem cells.[12] Loss of *Ewsr1* also leads to a block in brown fat development.[6] Although the loss of EWSR1 function has been demonstrated in an animal model, the role of EWSR1 in cellular senescence or the molecular action mechanisms of EWSR1 in cellular processes such as macroautophagy (autophagy) has not been fully elucidated.

Autophagy is an evolutionarily conserved self-digestive process that contributes to cellular homeostasis in a range of organisms from yeast to mammals.[13,14] Autophagy is initiated when parts of the cytoplasm and damaged organelles are engulfed in double-membrane vacuoles, called autophagosomes. Following docking and fusion of the autophagosome and lysosome to form an autolysosome, the sequestered contents are degraded by activated lysosomal hydrolases.[13,14] Under stress conditions, autophagy often plays a key role by removing damaged organelles and recycling nutrients and energy within the cell.[15-17] Conversely, excessive or deficient autophagy may result in various diseases, including neurodegenerative disorders and cancer.[15,16,18,19]

MicroRNAs (miRNAs), small endogenously expressed noncoding RNAs (~22 nucleotides), regulate gene expression at the post-transcriptional level. MiRNAs can pair with partially complementary sites in the 3'UTR of target genes, resulting in mRNAs (mRNAs) degradation or translational repression. Long primary transcript miRNAs (called pri-miRNAs), originating from long primary transcripts, are processed in the nucleus by DROSHA, a member of the ribonuclease III family (RNase III), and converted into precursor miRNAs (pre-miRNAs). Then, the pre-miRNA is exported to the cytoplasm by XPO5/EXPORTIN-5 and is further processed by DICER1, another RNase III protein. One strand of the duplex is incorporated into the RNA-induced silencing complex.[20,21]

Even though miRNAs can regulate the expression of genes in numerous pathways, their targets and roles have not been fully defined. Importantly, a growing body of evidence indicates that miRNAs modulate autophagy.[22] For instance, miRNAs target members of *ATG*s and other autophagy regulators and negatively regulate their activities.[22] Furthermore, miRNAs modulate autophagy at different stages such as autophagic induction, vesicle nucleation, vesicle elongation, and completion via targeting autophagy complexes by different miRNAs.[22-24] Considering the significance of autophagy in pathological conditions including cellular senescence and tumorigenesis, a study on the regulation of autophagy by EWSR1, a multifunctional protein, may provide a better understanding of autophagic signaling pathway.

In the current study, we investigated how EWSR1 deficiency is linked to autophagy and explored how EWSR1 regulates autophagy-related cellular processes using whole transcriptome (mRNA) sequencing combined with miRNA arrays to analyze genes and miRNAs that are significantly altered in *ewsr1*$^{-/-}$ MEFs. We further identified the transcriptome directly targeted by miRNAs involved in the autophagy pathway. We discovered that *Mir351* and *Mir351* directly target *Uvrag* and regulate autophagy through a post-transcriptional regulatory mechanism. We further confirmed that reduced UVRAG leads to autophagy inhibition in *Ewsr1* deficiency. Our results indicate that EWSR1 plays a novel role in the modulation of autophagy via miRNA-dependent pathway.

Results

Autophagy is altered by *Ewsr1*-deficiency

In order to examine whether EWSR1 deficiency is associated with autophagy, we used transmission electron microscopy to monitor direct evidence of autophagy in *Ewsr1*$^{+/+}$ vs. *ewsr1*$^{-/-}$ MEFs (**Fig. S1**). Indeed, ultrastructural images showed that autophagic vacuoles, including autophagosomes and autolysosomes, are significantly increased in *Ewsr1*$^{+/+}$ MEFs compared to *ewsr1*$^{-/-}$ MEFs. Furthermore, western blot analysis showed that the levels of LC3-II and UVRAG were decreased while the levels of endogenous BECN1, and ATG12–ATG5 conjugates, and SQSTM1/p62 (sequestome 1) were increased in *ewsr1*$^{-/-}$ MEFs (**Fig. 1A**).

In mammalian cells, most ATG proteins (eq. ULK1/2, BECN1, ATG12, ATG16L1, and LC3) are observed on phagophores, whereas only LC3 is found in autophagosome.[25] LC3 is cleaved by a cysteine protease, ATG4, and converted to LC3-I and subsequently conjugated to phosphatidylethanolamine to form LC3-II. Finally, LC3-II is localized in phagophore and autophagosome membranes.[25] LC3-II is a major marker for autophagy.[25] In this context, we found that the ratio of LC3-II to ACTB expression (LC3-II/ACTB) was significantly lower in *ewsr1*$^{-/-}$ MEFs compared to *Ewsr1*$^{+/+}$ MEFs ($P < 0.05$) (**Fig. 1B**). We further performed fluorescence microscopy to determine punctate structures of green fluorescent protein (GFP) conjugated to LC3 (GFP-LC3) that primarily represent autophagosomes.[25] As shown in **Fig. S2**, the number of punctate GFP-LC3 signals was significantly decreased in *ewsr1*$^{-/-}$ MEFs compared to *Ewsr1*$^{+/+}$ MEFs. Interestingly, SQSTM1 which serves as a link between LC3 and ubiquitinated substrates,[25] was increased in *ewsr1*$^{-/-}$ MEFs compared to *Ewsr1*$^{+/+}$ MEFs, implying that autophagic flux is altered. Autophagic flux means the degradation of substrates in the combined autophagosome and lysosome and is determined by the LC3 turnover assay.[25] To confirm autophagic flux in both *Ewsr1*$^{+/+}$ and *ewsr1*$^{-/-}$ MEFs, we performed SQSTM1 and LC3 turnover assays. In the turnover assay, chloroquine (CQ, a lysosomotropic agent) or E64d (a membrane-permeable cysteine protease inhibitor) and pepstatin A (Pep.A, an inhibitor of aspartic proteinases such as PGA/pepsin, CTSD, and CTSE) were used to prevent lysosomal degradation in intact cells.[26] As shown in **Figure 1C and D**, the treatment of CQ or E64d plus Pep.A increased LC3-II/ACTB ratio in both *Ewsr1*$^{+/+}$ and *ewsr1*$^{-/-}$ MEFs but the amount of LC3-II lipidation was relatively lower in *ewsr1*$^{-/-}$ MEFs than in *Ewsr1*$^{+/+}$ MEFs, indicating less autophagic flux in *ewsr1*$^{-/-}$ MEFs. A significant increase in the SQSTM1 levels following the treatment with E64d+Pep.A and CQ was detected in *Ewsr1*$^{+/+}$ MEFs compared to *ewsr1*$^{-/-}$ MEFs ($P < 0.05$) (**Fig. S3 and S4**). In order to further investigate whether CQ properly inhibits the turnover of autophagy substrates, cells were treated with 20 μM CQ for 6 h and 24 h, and 2 separate cell lysates were obtained in

0.5% Triton X-100-soluble and -insoluble fractions, respectively. Western blot analysis detected diffuse or free form of SQSTM1 from detergent (0.5% Triton X-100)-soluble lysate and SQSTM1 aggregates, a form of SQSTM1 oligomerization from detergent-insoluble fraction.[25] Our data showed that both increased levels of SQSTM1 and LC3-II by CQ treatment were

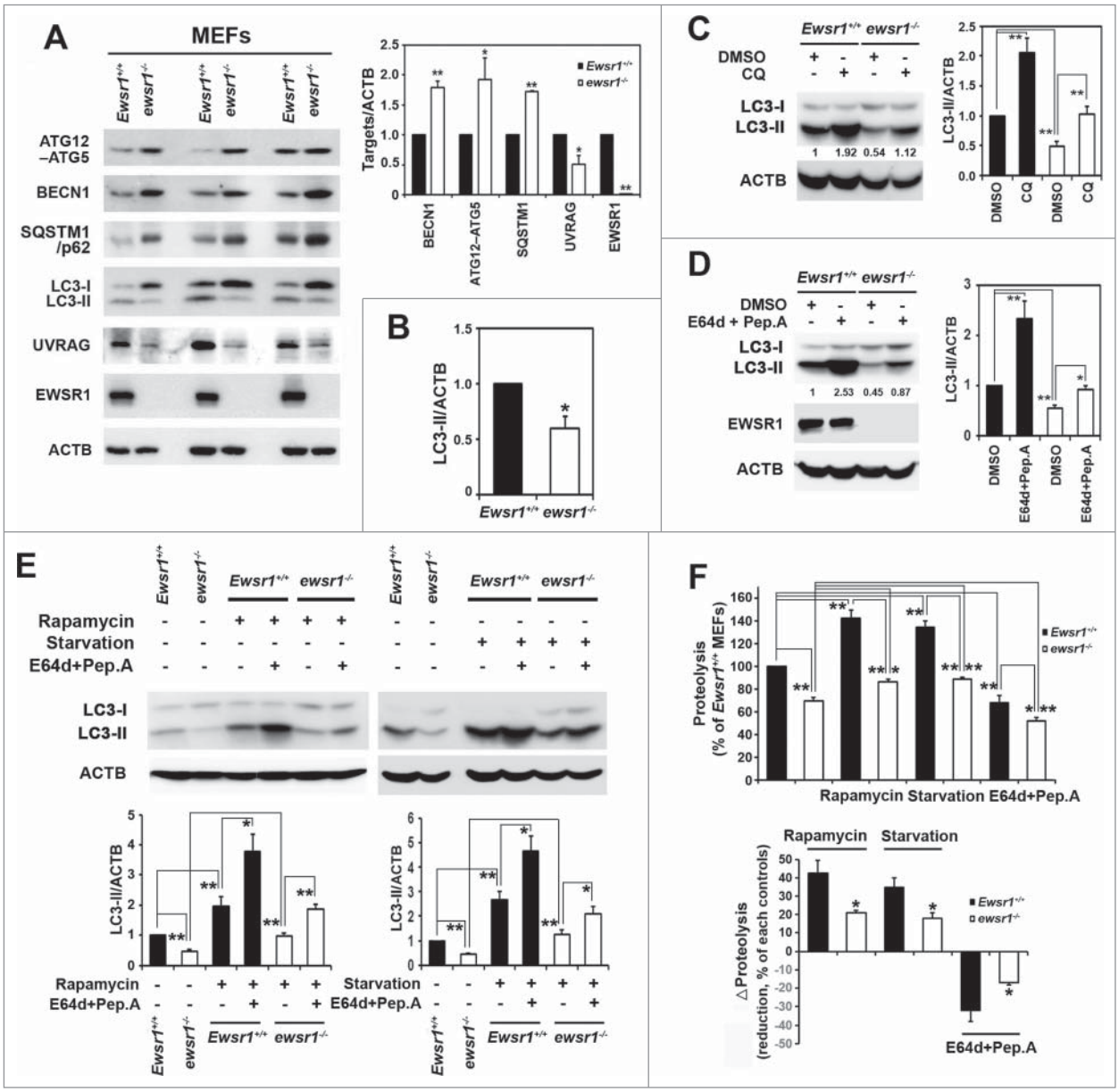

Figure 1. Autophagy is altered in *Ewsr1*-deficient MEFs. (**A**) Western blot analysis showed that endogenous BECN1, ATG12–ATG5 conjugates, and SQSTM1 but not LC3-II and UVRAG are elevated in *ewsr1*$^{-/-}$ MEFs. Blots are representative of 3 independent experiments. Densitometric analysis represents the mean ± SEM (n = 3; **P* < 0.05, ***P* < 0.005). (**B**) The decreased level of LC3-II indicated that autophagic activity is lower in *ewsr1*$^{-/-}$ MEFs than in *Ewsr1*$^{+/+}$ MEFs. These data were analyzed from western blot densitometric assessments (**A**) by normalizing LC3-II with ACTB as a loading control. Densitometric analysis represents the mean ± SEM (n = 3; **P* < 0.05, ***P* < 0.005). (**C**) LC3 turnover assay showed that autophagic flux is increased in *ewsr1*$^{-/-}$ MEFs in comparison to *Ewsr1*$^{+/+}$ MEFs. Cells were treated with 20 μM CQ for 6 h. Densitometric analysis represents the mean ± SEM (n = 5; **P* < 0.05, ***P* < 0.005). (**D**) The autophagic flux was differently regulated in *ewsr1*$^{-/-}$ MEFs in comparison to *Ewsr1*$^{+/+}$ MEFs. Cells were treated with 10 μg/ml E64d and 10 μg/ml Pep.A for 6 h. Densitometric analysis represents the mean ± SEM (n = 3; **P* < 0.05, ***P* < 0.005). (**E**) The induction of autophagy by rapamycin or starvation was differently regulated in in *ewsr1*$^{-/-}$ MEFs. Cells were incubated under treatment with 500 nM rapamycin or starvation for 24 h and then cells were treated with 10 μg/ml E64d and 10 μg/ml Pep.A for 6 h. Densitometric analysis represents the mean ± SEM (n = 3; **P* < 0.05, ***P* < 0.005). (**F**) A long-lived protein degradation assay showed that *Ewsr1* deficiency reduces lysosomal protein degradation. *Ewsr1* MEFs were labeled with L-[^{14}C] valine for 24 h, and degradation of long-lived proteins during incubation in each labeled conditions or complete medium was measured as described in Materials and Methods. Long-lived protein degradation is expressed as a percentage of the value obtained from untreated cells. The data represent the mean ± SEM (**P* < 0.05, ***P* < 0.005).

detected in detergent-soluble fraction from *Ewsr1*$^{+/+}$ MEFs (**Fig. S4**). Importantly, CQ treatment increased SQSTM1 aggregates in the detergent-insoluble fraction of both *Ewsr1* MEFs. Interestingly, CQ-induced SQSTM1 aggregates were markedly elevated in a time-dependent manner in the detergent-insoluble fraction of *Ewsr1*$^{+/+}$ MEFs. In contrast, CQ-induced SQSTM1 aggregates were lower and it was less time-dependent in the detergent-insoluble fraction of *ewsr1*$^{-/-}$ MEFs than in *Ewsr1*$^{+/+}$ MEFs. Collectively, as a result of CQ treatment for 24h, the total level of SQSTM1 was robustly increased in *Ewsr1*$^{+/+}$ MEFs compared to *ewsr1*$^{-/-}$ MEFs (**Fig. S4**).

Next, we further performed the LC3 turnover assay under rapamycin, a specific inhibitor of MTOR (mechanistic target of rapamycin), or starvation-stimulated autophagy activation in *Ewsr1* MEFs. Increased autophagic flux was confirmed by the above stimuli in both *Ewsr1*$^{+/+}$ and *ewsr1*$^{-/-}$ MEFs but the increase in the LC3-II/ACTB ratio was comparably lower in *ewsr1*$^{-/-}$ MEFs than in *Ewsr1*$^{+/+}$ MEFs ($P < 0.05$) (**Fig. 1E**). Additionally, a long-lived protein degradation assay[26] confirmed the expected stimulatory effects of rapamycin and starvation and inhibitory effect of E64d plus Pep.A on autophagic flux both *Ewsr1*$^{+/+}$ and *ewsr1*$^{-/-}$ MEFs. In all conditions, the amounts of long-lived protein degradation was significantly higher in *Ewsr1*$^{+/+}$ MEFs than in *ewsr1*$^{-/-}$ MEFs ($P < 0.05$) (**Fig. 1F**). Taken together, these data imply that the autophagic flux accompanying autophagy process is hindered by EWSR1 deficiency.

Uvrag is among the autophagy-related genes downregulated by *Ewsr1* deficiency

To identify autophagy-related genes affected by *Ewsr1* deficiency, we performed whole transcriptome sequencing (RNA-seq) and analyzed gene profiles in *Ewsr1*$^{+/+}$ MEFs and *ewsr1*$^{-/-}$ MEFs. Interestingly, *Uvrag* was decreased by nearly 2-fold in *ewsr1*$^{-/-}$ MEFs compared to *Ewsr1*$^{+/+}$ MEFs while most other autophagy-related genes (such as *Atg3*, *Atg10*, *Atg14*, *Map1lc3b*, and *Sqstm1*) were slightly increased (**Fig. 2A and B**). To validate the transcriptome data, several sets of qRT-PCR analysis were performed to detect mRNA levels of the 7 candidate genes including *Uvrag*. *Uvrag* mRNA was significantly decreased (> 2-fold) in *ewsr1*$^{-/-}$ MEFs compared to *Ewsr1*$^{+/+}$ MEFs ($P < 0.05$) (**Fig. 2C**). The downregulation of *Uvrag* mRNA was concurrent with the western blot data, which showed reduced UVRAG protein in *ewsr1*$^{-/-}$ MEFs (**Figs. 1A and 2C**). We further performed immunofluorescence staining and confocal microscopy and found a reduced UVRAG immunoreactivity in *ewsr1*$^{-/-}$ MEFs (**Fig. 2D**).

Reduction of *Uvrag* by *Ewsr1* deficiency leads to deregulation of autophagy

In order to confirm whether EWSR1 deficiency is associated with reduction of autophagic flux, we performed the LC3 turnover assay under the condition of EWSR1 knockdown by RNA interference in wild-type MEFs. As shown in **Figure 3A**, knockdown of EWSR1 decreased the basal level of autophagy as well as autophagic flux. Moreover, we confirmed that rapamycin or starvation-stimulated autophagy and autophagic flux were reduced by small interfering RNA (siRNA) targeting *Ewsr1* (**Fig. 3B and C**). These data indicate that EWSR1 deficiency is linked to the deregulation of autophagy.

It is quite clear that UVRAG is directly involved in autophagy.[27-29] In this context, to identify whether UVRAG plays a functional role in EWSR1 deficiency-linked deregulation of autophagy, we examined UVRAG gain and loss of function. As we expected, *Uvrag* overexpression increased autophagic activity while *Uvrag* knockdown using siRNA significantly reduced autophagic activity in both *Ewsr1*$^{+/+}$ and *ewsr1*$^{-/-}$ MEFs ($P < 0.05$) (**Fig. 3D and E**). Moreover, overexpression of UVRAG significantly elevated autophagic flux while *Uvrag* knockdown using siRNA significantly reduced autophagic flux ($P < 0.05$) (**Fig. 3F and G**). In order to check the off-target effects of siRNA targeting *Uvrag*, we transfected 4 different siRNA oligos respectively and verified their efficiency for *Uvrag* knockdown (**Fig. S5**). Most of *Uvrag*-specific siRNAs decreased the level of *Uvrag* and further reduced the level of LC3-II lipidation and autophagy flux upon E64d+Pep.A treatment (**Fig. S5**). Together, our data suggest that EWSR1 deficiency-linked deregulation of autophagy is mediated in a UVRAG-dependent manner.

Post-transcriptional *Ewsr1* regulates *Uvrag* expression at the post-transcriptional level

Since *Uvrag* mRNA was downregulated by *Ewsr1* deficiency, we proposed that EWSR1 may regulate the expression of *UVRAG*. To determine whether EWSR1 directly induces *Uvrag* gene expression, we ectopically expressed *Ewsr1* for 72 h and measured the protein levels of UVRAG (**Fig. 4A**). *Ewsr1*-transfected cells were harvested at the indicated time, and *Uvrag* mRNA was detected by RT-PCR. *Uvrag* mRNA was increased in parallel with *Ewsr1* mRNA in a time-dependent manner in *ewsr1*$^{-/-}$ MEFs ($P < 0.05$) (**Fig. 4A**). To examine the loss of EWSR1 function associated with UVRAG expression, siRNA targeting *Ewsr1* was transfected in both *Ewsr1*$^{+/+}$ MEFs and NIH 3T3 cells for 72 h. Knockdown of *Ewsr1* downregulated protein and mRNA levels of UVRAG ($P < 0.05$) (**Fig. 4B and C**). To confirm the post-transcriptional regulation of *Uvrag* by EWSR1, *Uvrag* mRNA in the nuclear fractions of *Ewsr1* MEFs were verified by reverse transcriptase PCR (RT-PCR). Notably, *Uvrag* exon levels were decreased in the cytosolic fraction to a greater degree than in the nuclear fraction (**Fig. 4D**). Because these results suggest that the expression of *Uvrag* is mainly regulated at the post-transcriptional level under EWSR1-deficiency conditions (**Fig. 4D**), we further addressed how and under what mechanism EWSR1 modulates UVRAG post-transcriptionally.

Uvrag is directly targeted by *Mir125a* and *Mir351*

We hypothesized that miRNAs may be involved in the post-transcriptional regulation of UVRAG under EWSR1-deficiency conditions. We performed microarray analysis of miRNA expression in both *Ewsr1*$^{+/+}$ and *ewsr1*$^{-/-}$ MEFs to identify miRNAs altered by EWSR1 deficiency and miRNAs that target *Uvrag* (**Fig. S6**). Interestingly, for the first time, we discovered that 2 miRNAs, *miR125a* and *miR351*, specifically target *Uvrag*. We performed functional enrichment analysis and found that 57

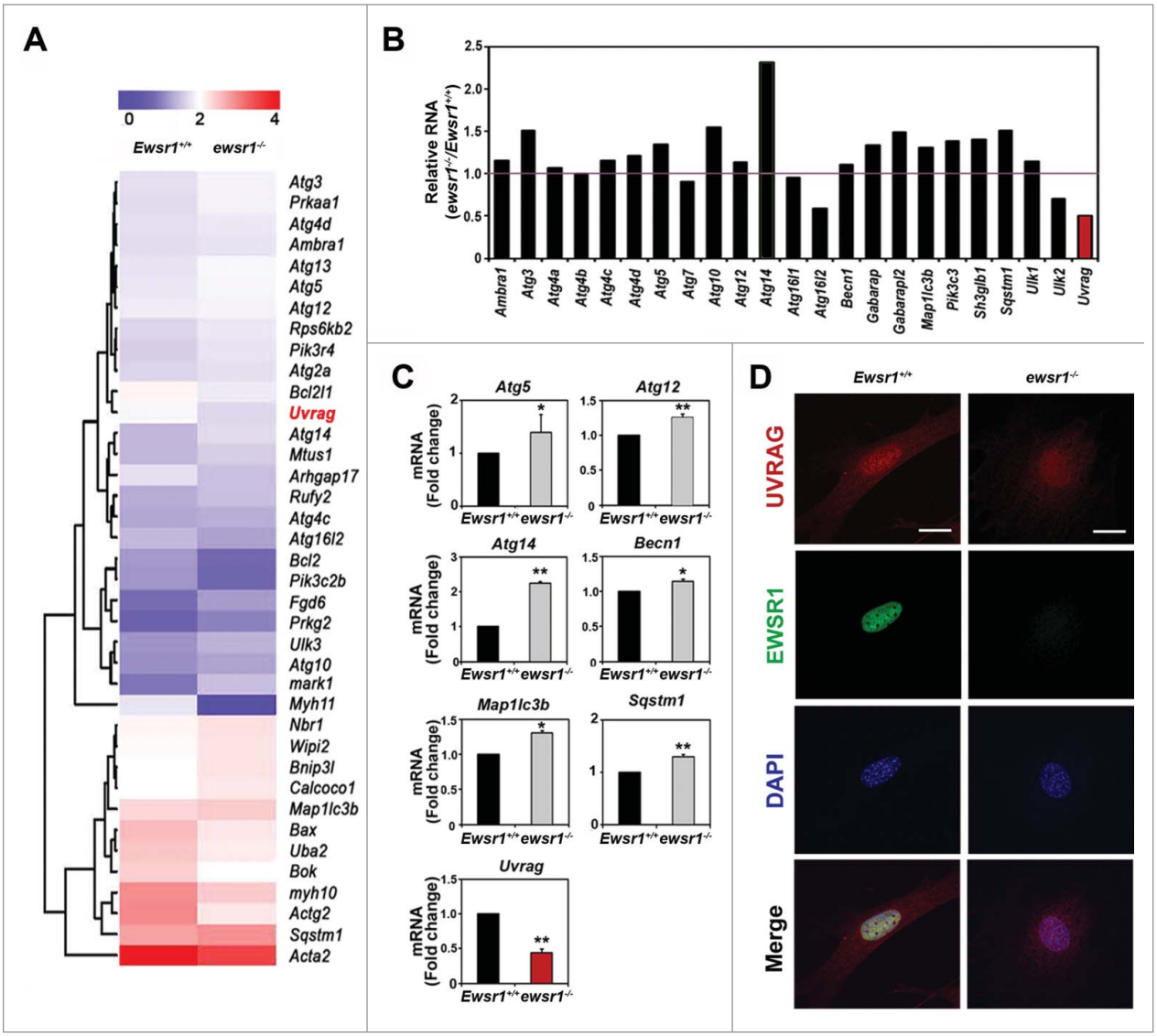

Figure 2. *Uvrag* is downregulated among autophagy-related genes in *Ewsr1*-deficient MEFs. (**A**) The heat map of the alteration of autophagy-related genes in *Ewsr1* MEFs explains that *Uvrag* is decreased in *ewsr1*$^{-/-}$ MEFs while other autophagy related genes are increased. Changes of gene expression are displayed by the colored bars as higher (red) or lower (purple). (**B**) Whole transcriptome sequencing (RNA-seq) and gene analysis showed that most autophagy-related genes but not *Uvrag* are increased slightly in *ewsr1*$^{-/-}$ MEFs. (**C**) qRT-PCR analysis confirmed that mRNA levels of most autophagy-related genes, but not *Uvrag* were significantly increased in *ewsr1*$^{-/-}$ MEFs (n = 3; *$P < 0.05$, **$P < 0.005$). (**D**) The immunoreactivity of UVRAG showed that UVRAG is decreased in *ewsr1*$^{-/-}$ MEFs. Scale bar (white): 10 μm.

genes among the 399 genes are involved in processes linked to autophagy and vesicle formation. We then generated a circulatory biological network to define relationships among the 59 genes and their associated processes as shown in **Figure 5A**. In addition, we specified the targeting of *Uvrag* by *Mir125a* and *Mir351* in the circulatory biological network (**Fig. 5A**). The identification of *Uvrag* 3'-UTR sequences targeted by *Mir125a* and *Mir351* were determined using TargetScan (http://www. targetscan.org). **Figure 5B** clearly illustrates that *Mir125a* and *Mir351* target complementary sequences (5'-CUCAGGGU-3') of the 3'UTR of *Uvrag*. The *Mir125a* and *Mir351* consensus sites for base paring on the 3'UTR of *Uvrag* have conserved homology among mammals including human and mouse (**Fig. 5C**). To further examine the post-transcriptional regulation of *Uvrag* by *Mir125a* and *Mir351*, pGL3-*Uvrag* 3'UTR reporter (luciferase) vector was cotransfected with *Mir125a* or *Mir351* in NIH 3T3 cells. Overexpression of *Mir125a* and *Mir351* significantly attenuated *Uvrag* 3'UTR luciferase activity ($P < 0.05$) (**Fig. 5D**). To verify whether mature forms of both miRNAs were derived from the pri-forms of miRNA, we performed RT-PCR analysis and detected the levels of pri-*Mir125a* and pri-*Mir351* in subcellular fractions (**Fig. 5E**). As we expected, levels of pri-*Mir125a* and pri-*Mir351* were significantly decreased in the nuclear factions of

ewsr1$^{-/-}$ MEFs, implying that pri-miRNAs are processed and converted into pre-miRNA in the nucleus by microprocessors. We further examined the levels of pre-*Mir125a* and pre-*Mir351* by qRT-PCR analysis. The pre-*Mir125a* and pre-*Mir351* were significantly increased in *ewsr1*$^{-/-}$ MEFs (right panel, $P < 0.05$) (**Fig. 5E**).

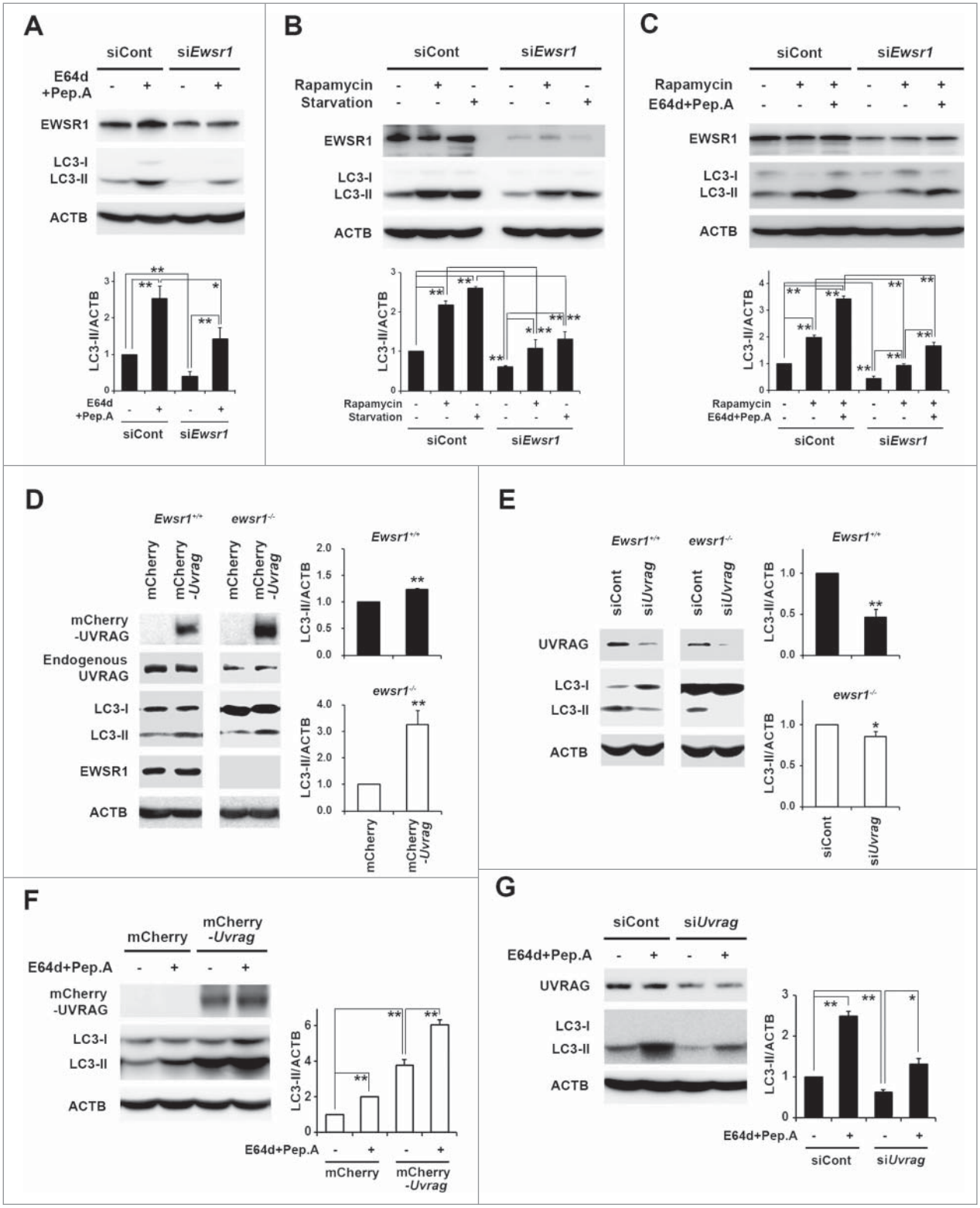

Figure 3. For figure legend, see page 802.

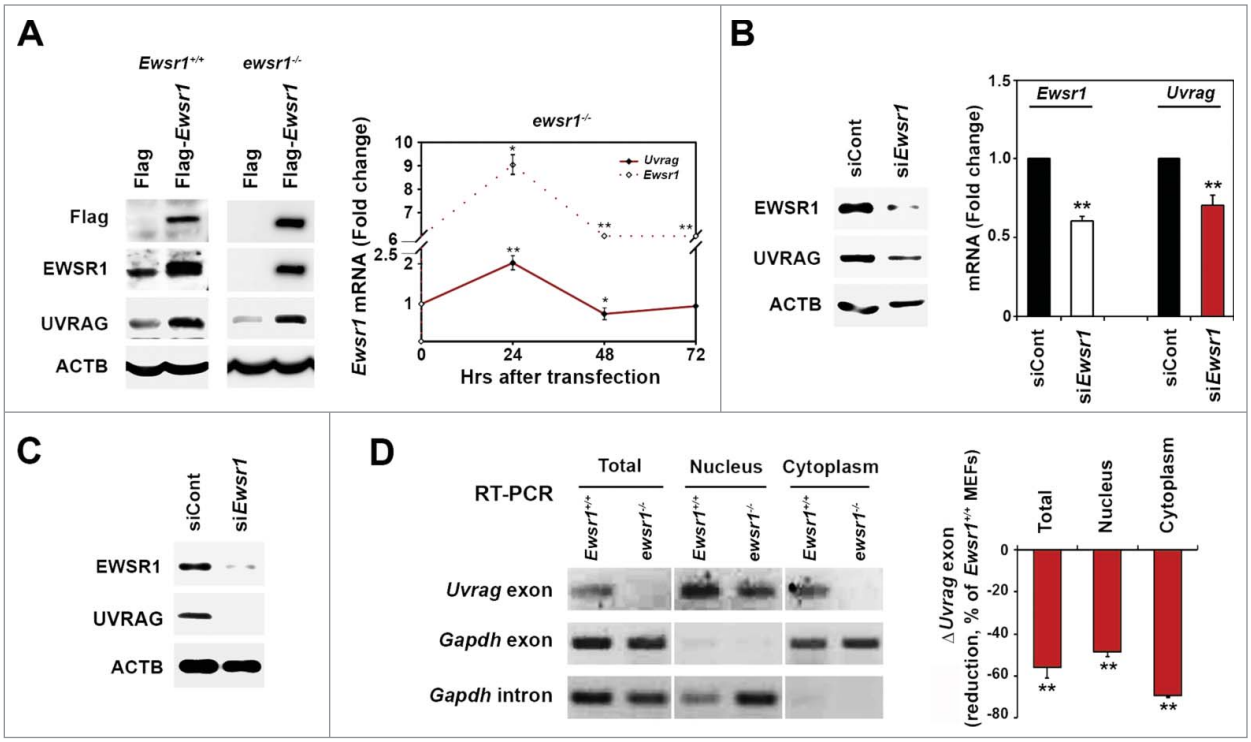

Figure 4. *Ewsr1* regulates the expression of *Uvrag* at the post-transcriptional level. (**A**) Western blot (left panel) and qRT-PCR analysis (right panel) showed that overexpression of *Ewsr1* increases protein and mRNA of UVRAG in MEFs. The graph data represent the mean ± SEM (n = 3; *$P < 0.05$, **$P < 0.005$). (**B**) Western blot (left panel) and qRT-PCR analysis (right panel) indicated that knockdown of *Ewsr1* decreases protein and mRNA of UVRAG in *Ewsr1*$^{+/+}$ MEFs. The graph data represent the mean ± SEM (n = 3; *$P < 0.05$, **$P < 0.005$). (**C**) Western blot analysis indicated that knockdown of *Ewsr1* decreases UVRAG in NIH 3T3 cells. (**D**) RT-PCR (left panel) and qRT-PCR analysis (right panel) demonstrated that the levels of the *Uvrag* exon is significantly decreased in the cytosol fraction in comparison to the nuclear fraction. The graph data represent the mean ± SEM (n = 3; *$P < 0.05$, **$P < 0.005$).

To confirm whether *Mir125a* and *Mir351* directly target *Uvrag*, we ectopically overexpressed both miRNAs and determined the protein and mRNA levels of UVRAG. Overexpression of *Mir125a* and *Mir351* resulted in significant downreguation of UVRAG in both *Ewsr1*$^{+/+}$ MEFs and NIH 3T3 cells ($P < 0.05$) (**Figs. 6A, B, and S7**). Importantly, both miRNAs reduced autophagy activity and autophagic flux as well (**Figs. 6B, C, and S7**). On the other hand, we designed *Mir125a*-specific antagomirs (Ant-*Mir125a*) and *Mir351*-specific antagomirs (Ant-*Mir351*) and tested whether the inhibition of endogenous *Mir125a* and *Mir351* affects the level of UVRAG and autophagy. We found that Ant-*Mir125a* and Ant-*Mir351* decreased *Mir125a* and *Mir351* levels, respectively, and significantly increased both UVRAG protein and autophagic flux compared to CNT-Ant transfected NIH 3T3 cells and *ewsr1*$^{-/-}$ MEFs ($P < 0.05$) (**Fig. 6D–I**). In order to confirm whether EWSR1 modulates the level of *Mir125a* and *Mir351*, we overexpressed *Ewsr1* and measured the level of *Mir125a* and *Mir351*

Figure 3 (See previous page). UVRAG is linked to the autophagy pathway under *Ewsr1*-deficiency conditions. (**A**) Knockdown of *Ewsr1* decreased autophagic flux in *Ewsr1*$^{+/+}$ MEFs. Cells were transfected for 72 h, with siRNA targeting *Ewsr1*, and then were treated with 10 μg/ml E64d and 10 μg/ml Pep.A for 6 h. Densitometric analysis represents the mean ± SEM (n = 5; *$P < 0.05$, **$P < 0.005$). (**B**) Knockdown of *Ewsr1* inhibited rapamycin or starvation-stimulated autophagy activation in *Ewsr1*$^{+/+}$ MEFs. Cells were treated for 72 h, with siRNA targeting *Ewsr1*, and then were incubated under rapamycin treatment or starvation for 24 h. Densitometric analysis represents the mean ± SEM (n = 3; *$P < 0.05$, **$P < 0.005$). (**C**) LC3 turnover assay indicated that knockdown of *Ewsr1* reduces autophagic flux in *Ewsr1*$^{+/+}$ MEFs. Cells were treated for 72 h, with siRNA targeting *Ewsr1*, and then were incubated under rapamycin treatment or starvation for 24 h. After that, E64d plus Pep.A were added for 6 h. Densitometric analysis represents the mean ± SEM (n = 4; *$P < 0.05$, **$P < 0.005$). (**D**) Overexpression of UVRAG positively regulated processing LC3-I to LC3-II in *Ewsr1* MEFs. Both cells were transfected with mCherry vector or mCherry-UVRAG for 48 h. Densitometric analysis represents the mean ± SEM (*Ewsr1*$^{+/+}$: n = 3, *ewsr1*$^{-/-}$: n = 7; *$P < 0.05$, **$P < 0.005$). (**E**) Knockdown of *Uvrag* decreased processing LC3-I to LC3-II in *Ewsr1*$^{+/+}$ MEFs. Both cells were transfected for 48 h with siRNA targeting *Uvrag*. Densitometric analysis represents the mean ± SEM (*Ewsr1*$^{+/+}$: n = 4, *ewsr1*$^{-/-}$: n = 5; *$P < 0.05$, **$P < 0.005$). (**F**) LC3 turnover assay showed that overexpression of UVRAG accelerates autophagic flux in *ewsr1*$^{-/-}$ MEFs. Cells were transfected with mCherry control vector or mCherry-UVRAG for 48 h and then E64d plus Pep.A were added for 6 h. Densitometric analysis represents the mean ± SEM (n = 4; *$P < 0.05$, **$P < 0.005$). (**G**) LC3 turnover assay showed that knockdown of UVRAG deceases autophagic flux in *Ewsr1*$^{+/+}$ MEFs. Cells were transfected for 48 h, with siRNA targeting *Uvrag* and then E64d plus Pep.A were added for 6 h. Densitometric analysis represents the mean ± SEM (n = 4; *$P < 0.05$, **$P < 0.005$).

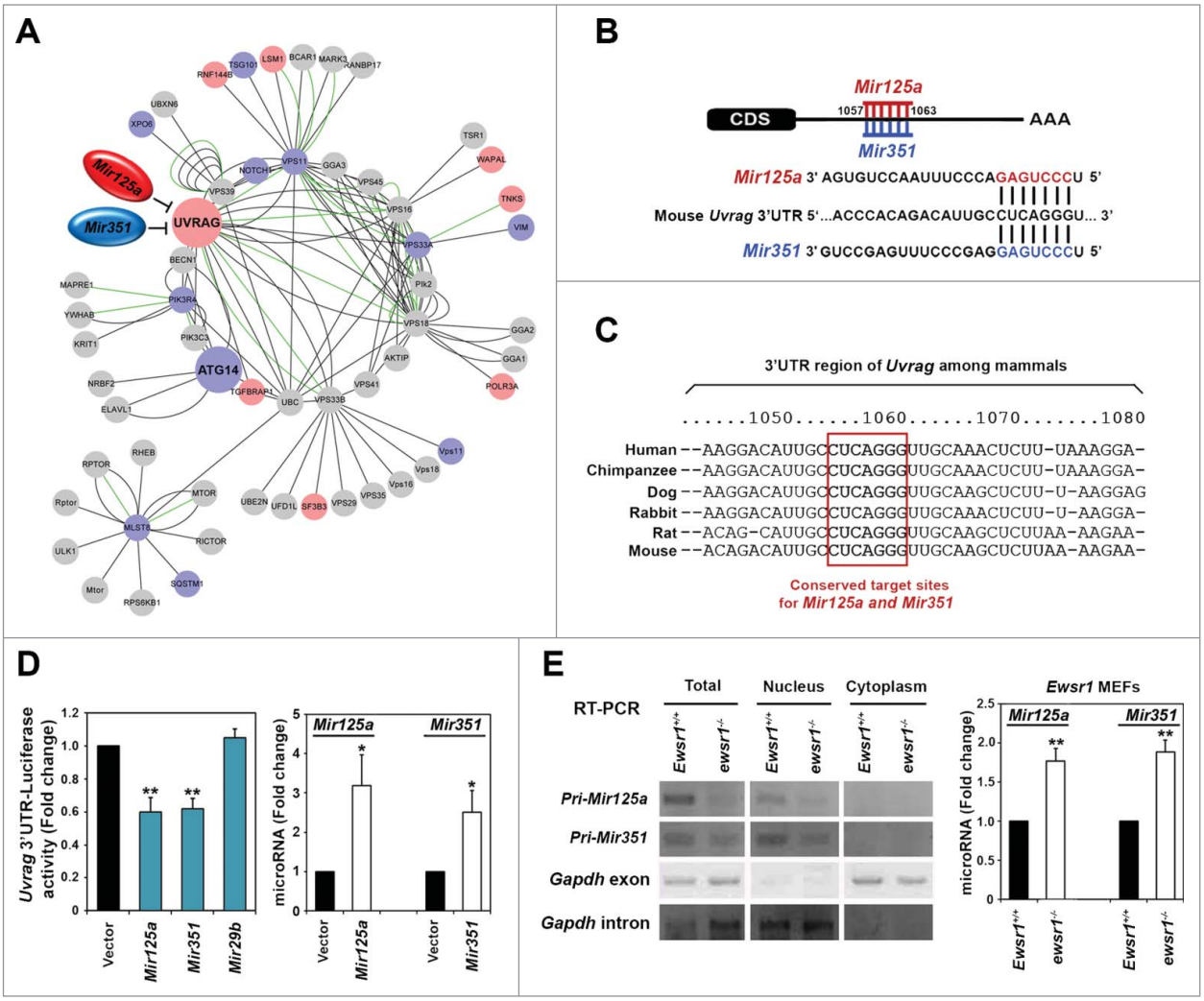

Figure 5. *Uvrag* is directly targeted by *Mir125a* and *Mir351*. (**A**) Protein-protein interaction network of 57 autophagy genes. A circulatory biological network delineating autophagy and vesicle pathway is represented by functionally enriched 57 genes. Light blue violet node denotes a gene whose mRNA expression level was increased (fold change>=1.5) in *ewsr1*$^{-/-}$ MEFs compared with *Ewsr1*$^{+/+}$ MEFs. Pale red denotes a gene whose mRNA expression level was decreased (fold change < 0.67). Gray nodes represent genes with no significant change in mRNA expression levels. The edges were defined based on interactions listed in NCBI Entrez Gene (http://www.ncbi.nlm.nih.gov/gene). Green edges denote that the source of the interaction information was Human Protein Reference Database (HPRD [http://www.hprd.org/]). Black edges denote that the source of the interaction information was BioGRID (http://thebiogrid.org). *Mir125a* (red) and *Mir351* (blue) target and act as the negative regulator of UVRAG. (**B**) *Uvrag* is a direct target of *Mir125a* and *Mir351*. The sequence alignments of *Mir125a* and *Mir351* and its target sites in the 3′UTR of *Uvrag*, downloaded from TargetScan (http://www. targetscan.org) are shown. (**C**) Schematic representation of conserved target sites for *Mir125a* and *Mir351* in the 3′UTR of *Uvrag* among mammals including human, chimpanzee, dog, rabbit, rat, and mouse. *Mir125a* and *Mir351* binding-target sequences in the 3′UTR of *Uvrag* were performed by TargetScan (http://www.targetscan.org) and was highlighted by the red box. (**D**) Overexpression of *Mir125a* and *Mir351* suppressed *Renilla* luciferase expression controlled by the *Uvrag* 3′UTR in NIH 3T3 cells, compared with vector control (left panel). *Mir29b* was used as a negative control. qRT-PCR analysis represented that overexpression with Ant-*Mir125a* and Ant-*Mir351* increased each mature *Mir351* and *Mir351* in NIH 3T3 cells (right panel). The graph data represent the mean ± SEM (n = 3; **P* < 0.05, ***P* < 0.005). (**E**) RT-PCR analysis demonstrated that the levels of pri-*Mir125a* and pri-*Mir351* are decreased in subcellular fractions of *Ewsr1* MEFs (left panel). The intron and exon of mouse *Gapdh* were amplified as markers of nuclear RNA and cytoplasmic RNA. qRT-PCR analysis revealed that *Mir125a* and *Mir351* were increased in *ewsr1*$^{-/-}$ MEFs (right panel). The graph data represent the mean ± SEM (n = 3; **P* < 0.05, ***P* < 0.005).

by qRT-PCR. Exogenous *Ewsr1* significantly reduced *Mir125a* and *Mir351* in *ewsr1*$^{-/-}$ MEFs ($P < 0.05$) (**Fig. 6J**). Together, these data provide a link that *Mir125a* and *Mir351* directly target and regulate *Uvrag* mRNA post-transcriptionally by EWSR1 deficiency, resulting in autophagy alteration.

Uvrag is controlled by the activity of microprocessors

We further investigated whether the miRNA processing machinery (DROSHA, DGCR8, DICER1, and AGO2) is involved in the biogenesis of *Mir125a* and *Mir351* and the subsequent regulation of *Uvrag* expression. Using whole transcriptome

analysis, we found that only *Drosha* is significantly increased in *ewsr1*$^{-/-}$ MEFs compared to *Ewsr1*$^{+/+}$ MEFs (**Fig. 7A and S8A**). To study the post-transcriptional regulation of *Uvrag*, we used pGL3-*Uvrag*-3'UTR vector. The post-transcriptional activity of *Uvrag* was monitored after treatment with either siRNAs (si*Drosha*, si*Dgcr8*, and si*Dicer1*) or constructs (FLAG vector, *Drosha*-FLAG, *Ago2*-FLAG, V5 vector, V5-*Dgcr8*, V5-*Dicer1*) cotransfected with pGL3-*Uvrag*-3'UTR vector. As shown in **Figure 7B and S8C**, knockdown of *Drosha*, *DGCR8*, and *Dicer1* significantly increased *Uvrag*-3'UTR luciferase activity, in

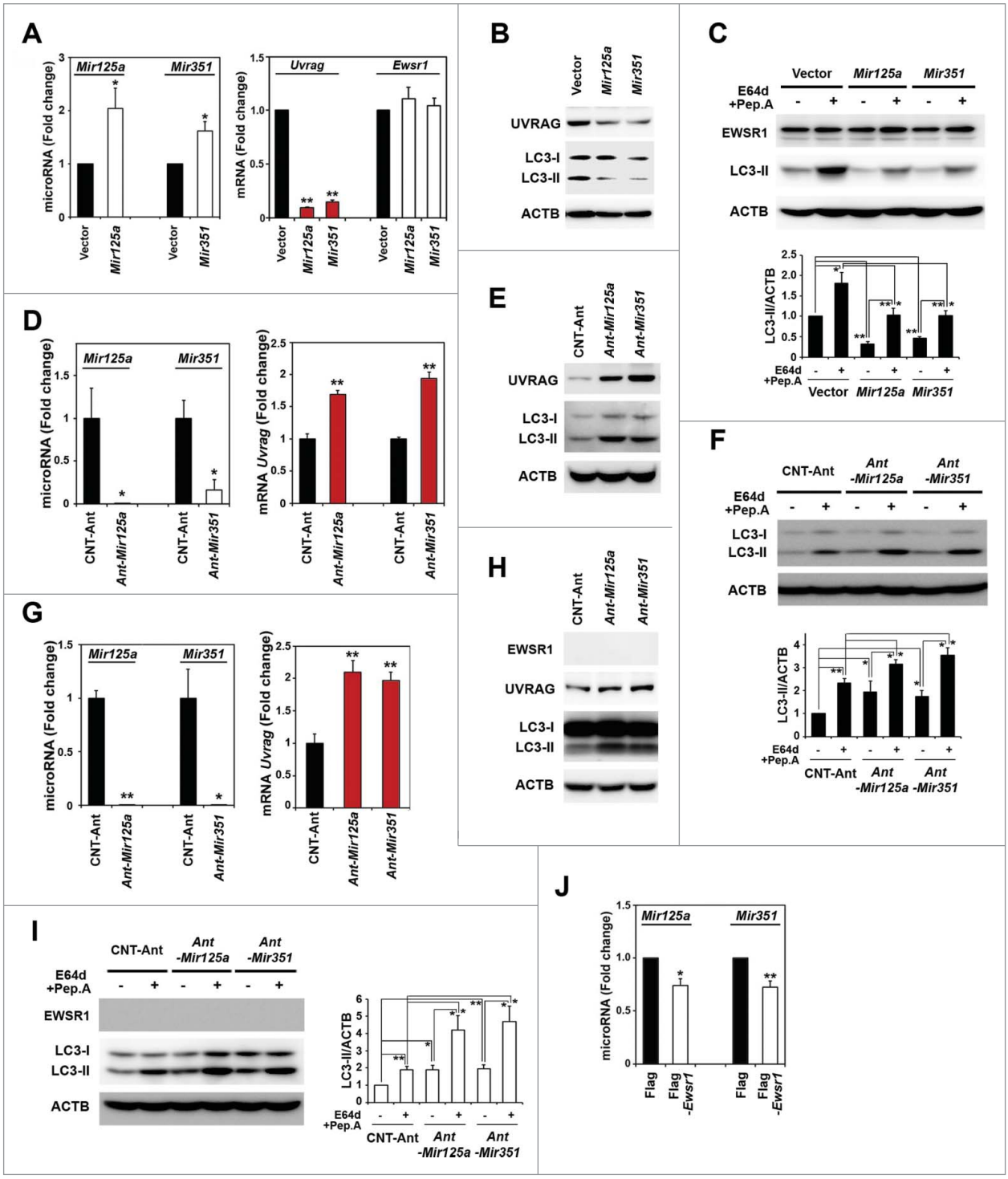

Figure 6. For figure legend, see page 805.

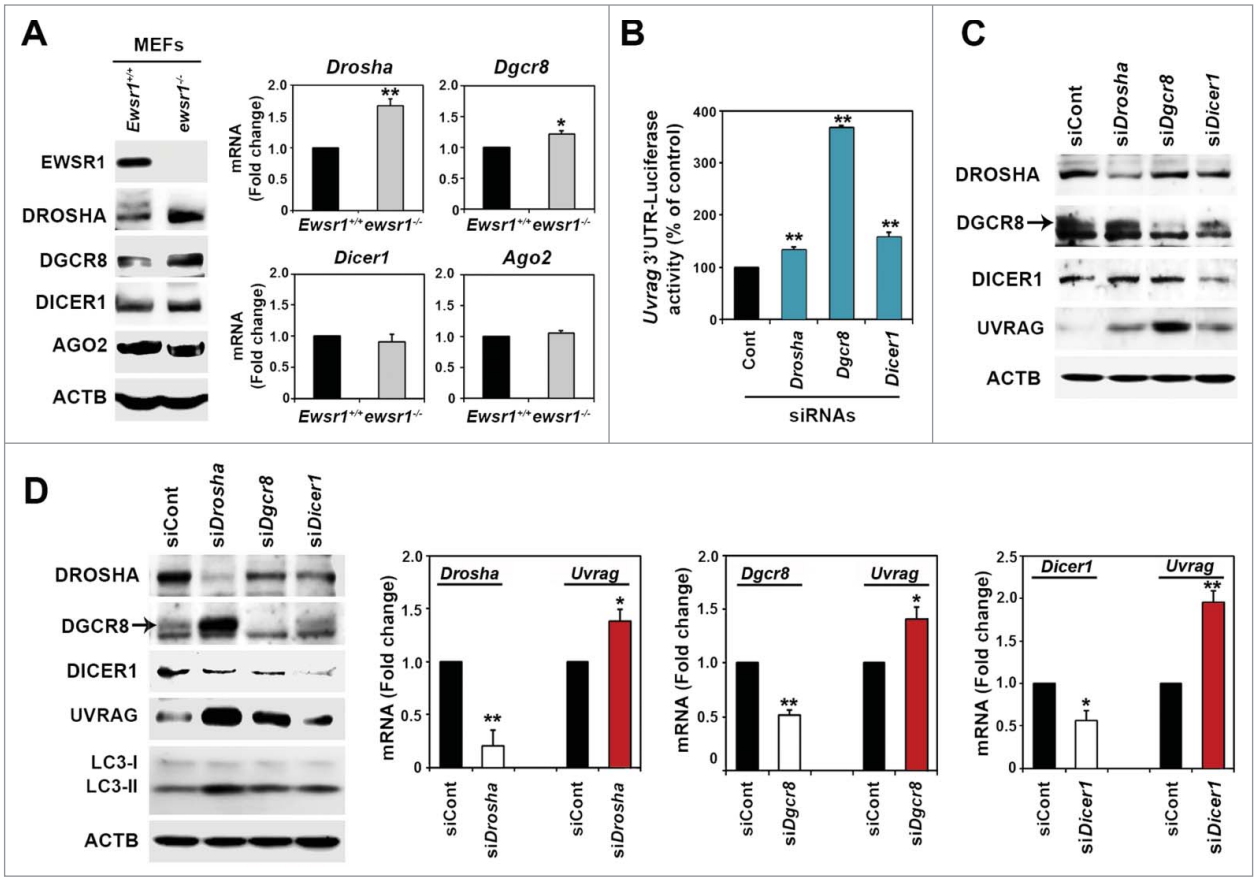

Figure 7. UVRAG is controlled by a microprocessor-dependent pathway. (**A**) Western blot and qRT-PCR analysis showed that DROSHA is increased in *ewsr1*$^{-/-}$ MEFs. DGCR8, DICER1, and AGO2 did not change significantly. The graph data represent the mean ± SEM (n = 3; **P* < 0.05, ***P* < 0.005). (**B**) Knockdown of *Drosha*, *Dgcr8*, or *Dicer1* significantly increased *Renilla* luciferase expression controlled by the *Uvrag* 3′UTR in NIH 3T3 cells, compared with control siRNA. NIH 3T3 cells were cotransfected with siRNAs targeting *Drosha*, *Dgcr8*, or *Dicer1* and pGL3-*Uvrag*-3′UTR vector for 72 h. The graph data represent the mean ± SEM (n = 3; **P* < 0.05, ***P* < 0.005). (**C**) Western blot analysis showed that knockdown of *Drosha*, *Dgcr8*, or *Dicer1* significantly increases UVRAG protein in NIH 3T3 cells, compared with control siRNA. NIH 3T3 cells were transfected with siRNAs targeting *Drosha*, *Dgcr8*, or *Dicer1* for 72 h. Blots are representative of 3 independent experiments. (**D**) Western blot and qRT-PCR analysis showed that knockdown of *Drosha*, *Dgcr8*, or *Dicer1* significantly increases UVRAG and autophagy in *ewsr1*$^{-/-}$ MEF, compared with control siRNA. Cells were transfected with siRNAs targeting *Drosha*, *Dgcr8*, or *Dicer1* for 72 h and then harvested. The graph data represent the mean ± SEM (n = 3; **P* < 0.05, ***P* < 0.005).

Figure 6 (See previous page). *Uvrag* is negatively regulated by *Mir125a* and *Mir351*. (**A**) qRT-PCR analysis represented that overexpression of *Mir125a* and *Mir351* downregulates the level of mRNA *Uvrag* in *Ewsr1*$^{+/+}$ MEFs. The graph data represent the mean ± SEM (n = 3; **P* < 0.05, ***P* < 0.005). (**B**) Western blot analysis demonstrated overexpression of *Mir125a* and *Mir351* downregulates both *Uvrag* and conversion of LC3-I to LC3-II in *Ewsr1*$^{+/+}$ MEFs. Blots are the representative of 3 independent experiments. (**C**) LC3 turnover assay showed that overexpression of *Mir125a* and *Mir351* reduces autophagic flux in *ewsr1*$^{-/-}$ MEFs. Cells were transfected for 72 h with vector control, *Mir125a*, or *Mir351*, and then E64d plus Pep.A were added for 6 h. Densitometric analysis represents the mean ± SEM (n = 3; **P* < 0.05, ***P* < 0.005). (**D**) qRT-PCR analysis represented that treatment with Ant-*Mir125a* and Ant-*Mir351* increases both mature *Mir125a* and *Mir351*, as well as *Uvrag* mRNA in NIH 3T3 cells. The graph data represent the mean ± SEM (n = 3; **P* < 0.05, ***P* < 0.005). (**E**) Western blot analysis demonstrated that treatment with Ant-*Mir125a* and Ant-*Mir351* increases both UVRAG and LC3-II in NIH 3T3 cells. Blots are representative of 3 independent experiments. (**F**) LC3 turnover assay showed that treatment with Ant-*Mir125a* and Ant-*Mir351* increases autophagic flux in NIH 3T3 cells. Cells were transfected for 72h with CNT-Ant, Ant-*Mir125a*, or *Mir125a*, and then E64d plus Pep.A were added for 6 h. Densitometric analysis represents the mean ± SEM (n = 3; **P* < 0.05, ***P* < 0.005). (**G**) qRT-PCR analysis showed that treatment with Ant-*Mir125a* and Ant-*Mir351* increases both mature *Mir125a* and *Mir351*, as well as *Uvrag* mRNA in *ewsr1*$^{-/-}$ MEFs. The graph data represent the mean ± SEM (n = 3; **P* < 0.05, ***P* < 0.005). (**H**) Western blot analysis indicated that treatment with Ant-*Mir125a* and Ant-*Mir351* increases both UVRAG and LC3-II in *ewsr1*$^{-/-}$ MEFs. Blots are representative of 3 independent experiments. (**I**) LC3 turnover assay demonstrated that treatment with Ant-*Mir125a* and Ant-*Mir351* increases autophagic flux in *ewsr1*$^{-/-}$ MEFs. Cells were transfected with CNT-Ant, Ant-*Mir125a*, or *Mir125a* for 72 h and then E64d plus Pep.A were added for 6 h. Densitometric analysis represents the mean ± SEM (n = 3; **P* < 0.05, ***P* < 0.005). (**J**) qRT-PCR analysis demonstrated that overexpression of *Ewsr1* reduces *Mir125a* and *Mir351* levels in *ewsr1*$^{-/-}$ MEFs. The graph data represent the mean ± SEM (n = 3; **P* < 0.05, ***P* < 0.005).

contrast to the microprocessors which significantly reduced the post-transcriptional activity ($P < 0.05$). UVRAG mRNA and protein were significantly increased after microprocessor knockdown in NIH 3T3 cells ($P < 0.05$) (**Fig. 7C and S8B**) and in *ewsr1*$^{-/-}$ MEFs ($P < 0.05$) (**Fig. 7D**). We also found that overexpression of the miRNA processing machinery negatively regulates UVRAG expression ($P < 0.05$) (**Fig. S8D**). These results demonstrate that microprocessors regulate *Uvrag* post-transcriptionally via the biogenesis of miRNA's.

Ewsr1 regulates UVRAG and autophagy in vivo

To verify whether our in vitro findings regarding the role of EWSR1 in the regulation of UVRAG and autophagy are replicable in vivo, we characterized UVRAG, *Mir125a*, *Mir351*, and autophagy in the skin of *Ewsr1* WT and *ewsr1* KO mice. Consistent with in vitro data, UVRAG protein and mRNA levels were significantly decreased in the skin of *ewsr1* KO compared to *Ewsr1* WT mice (right panel, $P < 0.05$) (**Fig. 8A**). Notably, *Mir125a* and *Mir351* levels were significantly increased in the skin of *ewsr1* KO mice ($P < 0.05$) (**Fig. 8B**). These results imply that UVRAG is regulated by EWSR1 in vivo. Interestingly, LC3-II was significantly reduced in *ewsr1* KO mice compared to *Ewsr1* WT controls ($P < 0.05$) (**Fig. 8A**). The in vivo monitoring of autophagic flux in animal models is currently not possible so we cannot compare results to our in vitro studies using intact cells.[26] Even though we could not confirm in vivo autophagic flux in the skin using turnover assay, our data indicate clearly that autophagic activity is decreased in the skin of *ewsr1* KO mice. Cresyl violet (Nissl) staining showed morphological changes in the skin of *ewsr1* KO mice compared to *Ewsr1* WT mice (**Fig. 8C**). UVRAG immunoreactivity was decreased in the skin of *ewsr1* KO mice (**Fig. 8C**). These data suggest that alterations of UVRAG and the autophagy pathway by EWSR1 deficiency may be linked to deregulation of cellular function.

Discussion

In the current study, we determined how EWSR1 is linked to autophagy pathways using *ewsr1* KO MEFs and mice and made 2 novel findings. First, *Ewsr1* deficiency leads to upregulation of microprocessor complexes as well as *Mir125a* and *Mir351*. Notably, EWSR1 indirectly targets UVRAG protein expression at the post-transcriptional level via *Mir125a* and *Mir351*. Second, *Ewsr1* deficiency is associated with an aberrant deregulation of autophagy pathway. Reduced levels of *Uvrag* mRNA and protein are linked to the altered autophagy pathway in *ewsr1* KO mice.

Ewsr1 modulates *Uvrag* at the post-transcriptional level via *Mir125a* and *Mir351*

Uvrag, which was initially discovered in a genetic screen for rescuing the UV sensitivity in xeroderma pigmentosum (XP) cells,[30] is a mammalian ortholog of yeast Vps38 and a promoter of autophagy.[15,26] It forms distinct complexes with BECN1 (mammalian ortholog of yeast Vps30/Atg6) and the class III phosphatidylinositol 3-kinase (whose catalytic subunit [PIK3C3] is the mammalian ortholog of yeast Vps34) and contributes to both autophagosome formation and maturation.[26] Interestingly, UVRAG is known as a tumor suppressor and suppresses cancer cell growth by promoting autophagy. UVRAG deficiency decreases autophagy and raises uncontrolled cell proliferation.[26] On the other hand, UVRAG plays a critical role in protecting cancer cells against apoptotic stimuli through regulation of BAX mitochondrial localization and preventing them from accumulating abnormal chromosomes.[31,32]

To date it has not been established whether EWSR1 participates in the post-transcriptional regulation of UVRAG expression via DROSHA and miRNA-dependent pathways. Interestingly, we discovered that *Uvrag* mRNA is mainly regulated in the cytoplasm and is inversely correlated with elevated DROSHA levels in *ewsr1*$^{-/-}$ MEFs. DROSHA is a miRNA processor and plays a pivotal role in miRNA maturation from pri-miRNA to pre-miRNA.[33] Because DROSHA is increased by EWSR1 deficiency,[34] we hypothesized that UVRAG levels may be modulated by a DROSHA-miRNAs-dependent pathway. We performed miRNA microarray analyses and identified that *Mir125a* and *Mir351* are significantly increased in *ewsr1*$^{-/-}$ MEFs. Indeed, for the first time, we verified that *Uvrag* mRNA is a direct target of *Mir125a* and *Mir351*. It has been shown that *Mir125a* targets genes such as *TNFAIP3* (tumor necrosis factor, α-induced protein 3),[35] *Dlg4/PSD-95* (discs, large homolog 4 (Drosophila)),[36] *BAK1* (BCL2-antagonist/killer 1),[37] and *TP53* (tumor protein p53).[38] In addition, *Mir351* targets *TMEM59* (transmembrane protein 59)[39] and *E2f3* (E2F transcription factor 3).[40] Even though Wang et al.[41] have proposed that *Uvrag* might be a potential target gene for *Mir351*, no study has proven or validated that possibility. Our data show that *Uvrag* is a direct target of both *Mir125a* and *Mir351* and that EWSR1 deficiency downregulates UVRAG via a miRNA-dependent pathway at the post-transcriptional level. Moreover, we confirmed that the levels of UVRAG and LC3-II (autophagy marker) are significantly reduced while the levels of *Mir125a* and *Mir351* are elevated in *ewsr1* KO mice. This in vivo finding support in vitro data that EWSR1 deficiency leads to a reduction of autophagy.

Ewsr1 deficiency is associated with the deregulation of autophagy pathway

UVRAG functions in both autophagy and endocytosis.[26,27] Liang et al.[26] show that overexpression of UVRAG increases proteolytically cleaved and lipidated MAP1LC3/LC3 (LC3-II). We confirmed this through functional studies (**Fig. 3**). Autophagy is initiated by the assembly of core BECN1 and PIK3C3 with BECN1-interacting proteins to form the autophagosome. The core complex exists in multiple forms with different BECN1-interacting proteins, UVRAG and ATG14, in a mutually exclusive manner.[42] The UVRAG-containing complex is responsible for the broad spectrum of cellular functions involved in early stage autophagy, late stage autophagosome maturation, autophagosome fusion with lysosome, and PIK3C3-related endocytic trafficking.[26,27] Recently, several papers have reported that UVRAG is directly involved in endocytic degradation through the role of the UVRAG-HOPS (homotypic fusion and protein

sorting) complex at a late step but not in autophagosome formation or autophagosome-lysosome fusion. [28,43-45] The direct role of UVRAG in autophagy is controversial, but our current data clearly show that a reduction of UVRAG contributes to the deregulation of autophagy in the context of *Ewsr1* deficiency even though ATG14, an alternative partner of UVRAG that

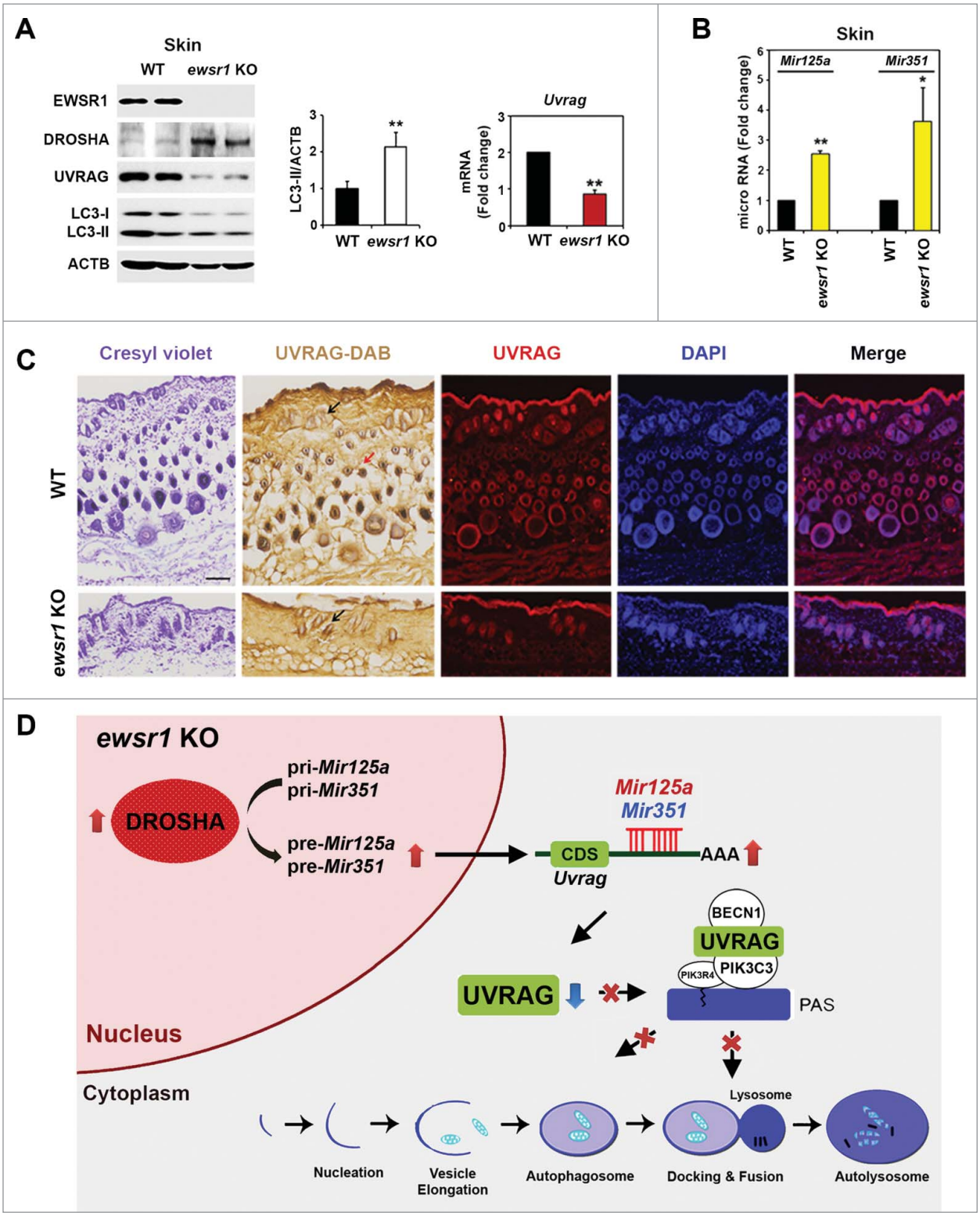

Figure 8. For figure legend, see page 808.

binds to BECN1, is highly expressed in the absence of *Ewsr1*. In general, ATG14-containing complexes participate in promoting autophagosome nucleation and expansion, resulting in early stage autophagosome biosynthesis.[46] Most intracellular ATG14 is present in a BECN1-dependent manner and the BECN1 and ATG14 complex can positively regulate autophagy through PIK3C3-PIK3R4.[28,42] Interestingly, we found that ATG14 and PIK3R4 were elevated (**Fig. 2A–C and S9A and B**) and, what is more, LAMP1/2 (lysosomal-associated membrane protein 1/2), and 4 types of lysosomal enzymes (cathepsins) were also increased in *ewsr1*$^{-/-}$ MEFs (**Fig. S9C–E**). It may be proposed that increased LAMPs and cathepsins accelerate autolysosomal protein degradation, implying enhancing autophagic flux and increased ATG14 plays a mechanistic role as a BECN1-binding partner to form the core complex of autophagy in lieu of UVRAG. However, it seems likely that increased ATG14 and the other molecules are not directly contributing to the deregulation of autophagy by *Ewsr1*-deficiency and UVRAG reduction. In this context, UVRAG is the major regulator of autophagy under *Ewsr1*-deficiency conditions. Taken together, our results conclude that the reduced level of UVRAG by *Ewsr1* deficiency deregulates autophagy and, in turn, it may contribute to cellular dysfunction in skin development.

In summary, our study provides evidence that *Ewsr1* modulates UVRAG at the posttranscription level (**Fig. 8D**). *Ewsr1* deficiency leads to an activation of DROSHA-mediated microprocessor complex and elevates the level of *Mir125a* and *Mir351* that directly target *Uvrag*. In addition, we discovered that altered UVRAG levels associated with *Ewsr1* deficiency lead to a novel cellular phenotype characterized as the deregulation of autophagy. The regulatory mechanism of UVRAG and autophagy by EWSR1 provides new insights into the role of *Ewsr1* deficiency-related cellular dysfunction. Thus, EWSR1-mediated regulation of UVRAG and autophagy may be a potential therapeutic target for restoration of the cellular function.

Materials and Methods

Plasmid construction

Mouse *Uvrag* (forward primer, 5'-ATGAGCTCCTGCGCCTCGCT-3' and reverse primer, 5'-TCACTTGTCGGAACTCCTGC-3') was amplified from *Ewsr1*$^{+/+}$ MEFs cDNA by PCR. The PCR product was cloned into mCherry (Clontech, 632522) with BamH I and Kpn I (New England BioLabs, R0136S and R0142S) restriction enzyme sites and sequenced. To generate the mouse *Uvrag* 3'UTR region in pGL4.14 with the *Xba* I (New England BioLabs, R0145S) restriction enzyme sites, the *Uvrag* 3'UTR was amplified by PCR (forward, 5′-GGCAGGCAGGCAGGCAGGCA-3′ and reverse primer, 5′-CAGGTCATGTGAAGTAAATT-3′) from *Ewsr1* MEFs cDNA and sequenced. *Mir125a* (forward primer, 5'-CGCGGATCCAAA AGGGTTTTTCTGGTCCA-3' and reverse primer, 5'-CCGCTCGAGGAGTTTCAAATGATG GTCAAG-3') and *Mir351* (forward primer, 5'-CGCGGATCCAAATGGCTGCTTTGTGACAT-3' and reverse primer, 5'-CCGCTCGAGAGGAAAGTGATTTTCACAGG-3') were amplified from *Ewsr1* MEFs cDNA by PCR. PCR product was cloned into pCDNA3 (Invitrogen Life Tech) with BamH I and Xho I (New England BioLabs, R0146S) restriction enzyme sites and sequenced.

Cell culture

Ewsr1 MEFs and NIH 3T3 cells were grown in Dulbecco's modified Eagle's medium (Hyclone, SH30243.01) supplemented with 10% fetal bovine serum (Hyclone, SH30071.03), 100 U/ml penicillin, 100 μg/ml streptomycin (Invitrogen Life Tech, 15070063). For culture of *Ewsr1* MEFs, 10% MEM nonessential amino acid solution (SIGMA, M7145) was added to the culture medium.

Western blot analysis

The cells were dispersed by pipetting in lysis buffer (10 mM Tris at pH 7.4, 1 mM ethylenediaminetetraacetic acid [EDTA], pH 8.0, 500 mM NaCl, and 0.5% Triton X-100 [Amresco, 0694]) and incubated for 30 min on ice. After centrifugation, the supernatant fraction was prepared as the Triton X-100-soluble fraction and the pellet fraction was used for the Triton X-100-insoluble fraction. Immunoblots were probed with the following antibodies: anti-ATG12–ATG5 (Novus Biologicals, NB110-53818), anti-BECN1 (Santa Cruz Biotechnology, sc-48381), anti-LC3 (Novus Biologicals, NB100-2220), anti-SQSTM1/p62 (Abcam, ab91526), anti-UVRAG (Millipore, AB2960), anti-EWSR1 (Santa Cruz Biotechnology, sc-28327), anti-FLAG (SIGMA, F3165), anti-DROSHA (AbCam, ab12286), anti-DGCR8 (provided by Dr. Narry Kim, Seoul National University),[20] anti-DGCR8 (Abcam, ab109098), anti-DICER1 (Santa Cruz Biotechnology, sc-30226), anti-AGO2 (Santa Cruz Biotechnology, sc-53521), anti-ACTB/β-ACTIN (ROCKLAND, RK600-401-886) and anti-TUBB3/TUBULIN (Millipore, 05-559), followed by treatment with the appropriate secondary antibodies conjugated to horseradish peroxidase

Figure 8 (See previous page). UVRAG is decreased in the skin of *ewsr1* KO mice. (**A**) Western blot (left panel) from skin tissues in *Ewsr1* WT and *ewsr1* KO mice showed that both UVRAG level and LC3 level are decreased while DROSHA level was increased in *ewsr1* KO mice. The autophagic activity (middle panel) was decreased in *ewsr1* KO mice. qRT-PCR analysis (right panel) confrimed that *Uvrag* mRNA was significantly decreased in *ewsr1* KO mice. The graph data represent the mean ± SEM (n = 3; **P* < 0.05). (**B**) qRT-PCR analysis indicated that the levels of *Mir125a* and *Mir351* are significantly increased in skin tissues of *ewsr1* KO mice. The graph data represent the mean ± SEM (n = 3; **P* < 0.05). (**C**) Cresyl Violet (Nissl) staining showed morphological changes in the skin between *Ewsr1* WT and *ewsr1* KO mice. UVRAG immunoreactivity was decreased in the skin of *ewsr1* KO mice. DAPI-stained nuclei are blue. Arrows are positive signals. Scale bars: 100 μm. (**D**) A schema illustrating the involvement of UVRAG in autophagy via post-transcriptional regulation under *Ewsr1*-deficient conditions. Upregulation of DROSHA by EWSR1 deficiency increases the processing of pri-miRNAs (pri-*Mir125a* and pri-*Mir351*) to pre-miRNAs. In turn, increased *Mir125a* and *Mir351* target and degrade *Uvrag* mRNA at the post-transcriptional level in the cytoplasm. As a result, EWSR1 deficiency leads to a reduction of UVRAG and deregulation of the UVRAG-dependent autophagy pathway.

(Pierce, 170-6515 and 170-6516). Immobilon™ Western ECL solution (Millipore, 34096) and a Kodak Image Station 4000MM (Kodak, 745280) were employed to visualize immunoreactive bands. ACTB or TUBB3 was used as the loading control.

Long-lived protein degradation assay

A long-lived protein degradation assay was performed with minor modifications to a previously reported protocol.[26,47] Briefly, cells were seeded at a concentration of 1.0×10^5 cells/cm2. After 18 h, 0.5 μCi/ml L-[^{14}C] valine (PerkinElmer, NEC291) was added for 24 h, the cells were washed 3 times in normal growth medium and incubated in normal growth medium supplemented with cold valine (5 mM) for 18 h. Thereafter, the cells were treated with autophagy activators or autophagy inhibitors as indicated. The growth medium was precipitated in 10% trichloroacetic acid (4°C for 10 min), centrifuged for 5 min at 15,000 g, and the supernatant fraction was collected. The cells were dissolved in 0.2 M NaOH (37°C for 10 min). The radioactivity in the supernatant fraction and in the dissolved cells was measured in a scintillation counter (Beckman, LS6500, Fullerton, CA, USA). Protein degradation was calculated by dividing the counts from the supernatant fractions with the total counts.

Whole transcriptome sequencing (RNA-seq) and gene analysis

For the mRNA-Seq sample preparation, the Illumina standard kit was used according to the manufacturer's protocol. Briefly, 3 μg of each total RNA sample was used for polyA mRNA selection using streptavidin-coated magnetic beads, followed by thermal mRNA fragmentation. The fragmented mRNA was subjected to cDNA synthesis using reverse transcriptase (SuperScript II; Toyobo, FSK101) and random primers. The cDNA was further converted into double stranded cDNA and, after an end repair process (Klenow fragment, T4 polynucleotide kinase and T4 polymerase), was finally ligated to Illumina paired end (PE) adaptors. Size selection was performed using a 2% agarose gel, generating cDNA libraries ranging in size from 200 to 250 bp. Finally, the libraries were enriched using 10 cycles of PCR and purified by the QIAquick PCR purification kit (Qiagen, 28106). The enriched libraries were diluted with Elution Buffer (Qiagen, 28106) to a final concentration of 10 nM. Each library was run at a concentration of 8 pM on one Genome Analyzer (GAIIx) (Illumina Inc. San Diego, CA, USA) lane using 53 bp sequencing. Reads were then processed and aligned to the mouse genome UCSC build mm9 using GSNAP.[48] GSNAP uses the normalized RNA-Seq 8 fragment counts to measure the relative abundances of transcripts. The unit of measurement is Reads Per Kilobase of exon per Million fragments mapped (RPKM).[49]

Transcriptional profile of autophagy/lysosomal genes

To visualize transcriptional profile of autophagy and lysosome-related genes, we selected genes related to autophagy or lysosome. Autophagy and lysosome-related genes were selected in terms of GO biological processes. The gene list was further filtered by using gene expression level information. Only genes with RPKM bigger than one were included. For autophagy-related genes, 15 upregulated genes with fold changes (*ewsr1*$^{-/-}$/*Ewsr1*$^{+/+}$) greater than 1.55 were selected and 12 downregulated genes with fold changes lower than 0.55 were selected. Additionally 11 genes that were known to be important in autophagy were selected. For lysosomal genes, 10 genes with fold changes greater than 1.4 were selected and 12 downregulated genes with fold changes lower than 0.7. Furthermore, 3 additional genes important in lysosomes are included. The RPKM expression values were log-transformed and the data was visualized with the *gplots* package in the R Development Core Team.

Quantitative real time-PCR (qRT-PCR)

Total RNA was extracted from *Ewsr1*$^{+/+}$ MEFs, *ewsr1*$^{-/-}$ MEFs and NIH 3T3 by TRIzol reagent (MRC, TR118). RNA was measured in a spectrophotometer at 260-nm absorbance. RNA analysis was conducted as follows: Fifty nanograms of RNA were used as a template for quantitative RT-PCR amplification, using SYBR Green Real-time PCR Master Mix (Toyobo, QPK-201). Primers were standardized in the linear range of cycle before the onset of the plateau. Primer sequences are given in Table S1. *Gapdh* was used as an internal control. Two-step PCR thermal cycling for DNA amplification and real-time data acquisition were performed with an ABI StepOnePlus™ Real-Time PCR System (Thermo Fisher Scientific, Waltham, MA, USA) using the following cycle conditions: 95°C for 1min × 1 cycle, and 95°C for 15 s, followed by 60°C for 1 min × 40 cycles. Fluorescence data were analyzed by the ABI StepOnePlus software and expressed as C_t the number of cycles needed to generate a fluorescent signal above a predefined threshold. The ABI StepOnePlus software set baseline and threshold values.

Confocal microscopy

Immunofluorescence staining and confocal microscopy was used to determine the localization and the immunoreactivity of UVRAG and EWSR1. Images were analyzed using a spinning disk confocal microscope (Olympus DSU, Tokyo, Japan).

RNA interference, antagomirs, and transfection

siGENOME SMARTpool Mouse *Uvrag* siRNA (L-064392-01-0005) and control nontargeting siRNA pool (D-001810-10-05) were purchased from Dharmacon (Chicago, IL, USA). A siRNA specific for mouse *Ewsr1* (5′-GACCACAGGAUGGUAACAATT-3′), *Drosha* (5′-AGAUCACCGUCUCUAGAAA-3′), *Ddgr8* (5′-AACAAUUUGGAGCUAGAUGAA-3′), and *Dicer1* (5′-ACACAGCAGUUGUCCUAAA-3′) were synthesized from COSMO GENETECH, Seoul, Korea. *Mir125a*-specific antagomirs (Ant-*Mir125a*, 5′-UCACAGGUUAAAGGGUCUCAGGGA-3′), *Mir351*-specific antagomirs (Ant-*Mir351*, 5-CAGGCUCAAAGGGCUCCUCAGGGA-3'), or control antagomirs (CNT-Ant, 5′-CAGUACUUUUGUGUAGUACAA-3′) were synthesized from COSMO GENETECH.

Ewsr1 MEFs and NIH 3T3 cells were transfected with 30 nM of all siRNAs or all antagomirs using RNAiMax transfection reagent (Invitrogen, 13778-150) according to the manufacturer's

instructions, cultured for 3 d, and then was collected for further experiments.

Subcellular fractionation

Harvested cells were washed with PBS and centrifuged at 108 g for 4 min at 4°C. The cell pellet was resuspended in 500 μl of ice-cold buffer (10 mM HEPES-KOH, pH 7.9, 1.5 mM $MgCl_2$, 10 mM KCl, 0.5 mM DTT and protease inhibitors [Sigma Aldrich, P2714]), kept on ice for 5 min and homogenized 20 times using a tight Dounce pestle. The homogenized sample was centrifuged at 1000 rpm for 5 min at 4°C to separate nuclei and other compartments. The supernatant fraction was retained as the cytoplasmic fraction. The pellet was resuspended in 300 μl of 0.25 M sucrose (Junsei, 31365-0301) buffer (containing 10 mM $MgCl_2$ [Sigma Aldrich, M4880]) and layered over 300 μl of 0.35 M sucrose buffer (containing 0.5 mM $MgCl_2$) and centrifuged at 2500 rpm for 5 min at 4°C. This step resulted in a separation of a cleaner nuclear fraction. Then, the nuclear fraction was resuspended in 300 μl of 0.35 M sucrose and sonicated 6 times, each time for 10 sec using a Bioruptor instrument (Diagenode Diagnostics, Liège, Belgium).

Reporter assay

NIH 3T3 cells were cultured in 48-well plates at a density of 5×10^4 cells per well, and the next day, cells were cotransfected with either siRNAs (si*Drosha*, si*Dgcr8*, and si*Dicer1*) or constructs (FLAG vector, *Drosha*-FLAG, *Ago2*-FLAG, V5 vector, V5-*Dgcr8*, V5-*Dicer1*) and pGL3-*Uvrag*-3'UTR vector. The luciferase activity was measured 72 h after the transfection.

Autophagy network

We generated a biological network to show the relationship of 57 genes related to *Uvrag* or *Atg14*. Genes that are related to *Uvrag* or *Atg14* according to the NCBI Entrez E-utility Web Service were candidates for network visualization. Genes with RPKM smaller than 1 in both *Ewsr1*$^{+/+}$ and *ewsr1*$^{-/-}$ MEFs were filtered out. The network is constructed with the remaining 57 genes using Cytoscape (v2.8.0).[50]

Histopathological evaluation

Serially cut skin tissue sections were immunostained for UVRAG using a previously reported conjugated secondary antibody method in skin tissue samples.[34] Preabsorption with excess target proteins, omission of the primary antibody, and omission of secondary antibodiy were performed to determine the amount of background generated from the detection assay.

Statistics

Data were obtained from least 3 independent experiments, and presented as the mean ± standard error of the mean (SEM). Statistical evaluation of the results was performed by the Student *t* test using SigmaPlot 2000 (Systat Software). Data were considered significant at a value of $P < 0.05$.

Disclosure of Potential Conflicts of Interest

No potential conflicts of interest were disclosed.

Acknowledgments

We thank Dr Jae U Jung for *Uvrag* constructs.

Funding

This study was supported by Brain Science Flagship Grant (2E24380 to HR) from Korea Institute of Science and Technology and NIH Grant (NS067283 to HR). This study was also supported by a grant from the National Research Foundation (NRF) of Korea (No. 2011-0030701 to YSK).

Supplemental Material

Supplemental data for this article can be accessed on the publisher's website.

References

1 Erkizan HV, Uversky VN, Toretsky JA. Oncogenic partnerships: EWS-FLI1 protein interactions initiate key pathways of Ewing's sarcoma. Clin Cancer Res 2010; 16:4077-83; PMID:20547696; http://dx.doi.org/10.1158/1078-0432.CCR-09-2261

2 Gascoyne DM, Thomas GR, Latchman DS. The effects of Brn-3a on neuronal differentiation and apoptosis are differentially modulated by EWS and its oncogenic derivative EWS/Fli-1. Oncogene 2004; 23:3830-40; PMID:15021903; http://dx.doi.org/10.1038/sj.onc.1207497

3 Araya N, Hirota K, Shimamoto Y, Miyagishi M, Yoshida E, Ishida J, Kaneko S, Kaneko M, Nakajima T, Fukamizu A. Cooperative interaction of EWS with CREB-binding protein selectively activates hepatocyte nuclear factor 4-mediated transcription. J Biol Chem 2003; 278:5427-32; PMID:12459554; http://dx.doi.org/10.1074/jbc.M210234200

4 Kovar H. Dr. Jekyll and Mr. Hyde: The Two Faces of the FUS/EWS/TAF15 Protein Family. Sarcoma 2011; 2011:837474; PMID:21197473; http://dx.doi.org/10.1155/2011/837474

5 Lee J, Rhee BK, Bae GY, Han YM, Kim J. Stimulation of Oct-4 activity by Ewing's sarcoma protein. Stem Cells 2005; 23:738-51; PMID:15917470; http://dx.doi.org/10.1634/stemcells.2004-0375

6 Park JH, Kang HJ, Kang SI, Lee JE, Hur J, Ge K, Mueller E, Li H, Lee BC, Lee SB. A multifunctional protein, EWS, is essential for early brown fat lineage determination. Dev Cell 2013; 26(4):393-404; PMID:23987512; http://dx.doi.org/10.1016/j.devcel.2013.07.002

7 Zucman J, Delattre O, Desmaze C, Epstein AL, Stenman G, Speleman F, Fletchers CD, Aurias A, Thomas G. EWS and ATF-1 gene fusion induced by t(12;22) translocation in malignant melanoma of soft parts. Nat Genet 1993; 4:341-5; PMID:8401579; http://dx.doi.org/10.1038/ng0893-341

8 Torchia EC, Boyd K, Rehg JE, Qu C, Baker SJ. EWS/FLI-1 induces rapid onset of myeloid/erythroid leukemia in mice. Mol Cell Biol 2007; 27:7918-34; PMID:17875932; http://dx.doi.org/10.1128/MCB.00099-07

9 Ladanyi M, Gerald W. Fusion of the EWS and WT1 genes in the desmoplastic small round cell tumor. Cancer Res 1994; 54:2837-40; PMID:8187063

10 Panagopoulos I, Hoglund M, Mertens F, Mandahl N, Mitelman F, Aman P. Fusion of the EWS and CHOP genes in myxoid liposarcoma. Oncogene 1996; 12:489-94; PMID:8637704

11 Li H, Watford W, Li C, Parmelee A, Bryant MA, Deng C, O'Shea J, Lee SB. Ewing sarcoma gene EWS is essential for meiosis and B lymphocyte development. J Clin Invest 2007;117:1314-23; PMID:17415412; http://dx.doi.org/10.1172/JCI31222

12 Cho J, Shen H, Yu H, Li H, Cheng T, Lee SB, Lee BC. Ewing sarcoma gene Ews regulates hematopoietic stem cell senescence. Blood 2011; 117(4):1156-66; PMID:21030557; http://dx.doi.org/10.1182/blood-2010-04-279349

13 Mizushima N, Levine B, Cuervo AM, Klionsky DJ. Autophagy fights disease through cellular self-digestion. Nature 2008; 451:1069-75; PMID:18305538; http://dx.doi.org/10.1038/nature06639

14 Glick D, Barth S, Macleod KF. Autophagy: cellular and molecular mechanisms. J Pathol 2010; 221:3-12; PMID:20225336; http://dx.doi.org/10.1002/path.2697

15 Maiuri MC, Zalckvar E, Kimchi A, Kroemer G. Self-eating and self-killing: crosstalk between autophagy and

apoptosis. Nat Rev Mol Cell Biol 2007; 8:741-52; PMID:17717517; http://dx.doi.org/10.1038/nrm2239
16 Portt L, Norman G, Clapp C, Greenwood M, Greenwood MT. Anti-apoptosis and cell survival: a review. Biochim Biophys Acta 2011; 1813:238-59; PMID:20969895; http://dx.doi.org/10.1016/j.bbamcr.2010.10.010
17 Levine B, Klionsky DJ. Development by self-digestion: molecular mechanisms and biological functions of autophagy. Dev Cell 2004; 6:463-77; PMID:15068787; http://dx.doi.org/10.1016/S1534-5807(04)00099-1
18 Huang J, Klionsky DJ. Autophagy and human disease. Cell Cycle 2007; 6:1837-49; PMID:17671424; http://dx.doi.org/10.4161/cc.6.15.4511
19 Kim Y, Kim YS, Kim DE, Lee JS, Song JH, Kim HG, Cho DH, Jeong SY, Jin DH, Jang SJ, et al. BIX-01294 induces autophagy-associated cell death via EHMT2/G9a dysfunction and intracellular reactive oxygen species production. Autophagy 2013; 9(12):2126-39; PMID:24322755; http://dx.doi.org/10.4161/auto.26308
20 Han J, Lee Y, Yeom KH, Kim YK, Jin H, Kim VN. The Drosha-DGCR8 complex in primary microRNA processing. Genes Dev 2004; 18:3016-27; PMID:15574589; http://dx.doi.org/10.1101/gad.1262504
21 Bratkovic T, Glavan G, Strukelj B, Zivin M, Rogelj B. Exploiting microRNAs for cell engineering and therapy. Biotechnol Adv 2012; 30:753-65; PMID:22286072; http://dx.doi.org/10.1016/j.biotechadv.2012.01.006
22 Fu LL, Wen X, Bao JK, Liu B. MicroRNA-modulated autophagic signaling networks in cancer. Int J Biochem Cell Biol 2012; 44:733-6; PMID:22342941; http://dx.doi.org/10.1016/j.biocel.2012.02.004
23 Liu B, Cheng Y, Liu Q, Bao JK, Yang JM. Autophagic pathways as new targets for cancer drug development. Acta Pharmacol Sin 2010; 31:1154-64; PMID:20694022; http://dx.doi.org/10.1038/aps.2010.118
24 Korkmaz G, le Sage C, Tekirdag KA, Agami R, Gozuacik D. miR-376b controls starvation and mTOR inhibition-related autophagy by targeting ATG4C and BECN1. Autophagy 2012; 8:165-76; PMID:22248718; http://dx.doi.org/10.4161/auto.8.2.18351
25 Mizushima N, Yoshimori T, Levine B. Methods in mammalian autophagy research. Cell 2010; 140:313-26; PMID:20144757; http://dx.doi.org/10.1016/j.cell.2010.01.028
26 Klionsky DJ, Abdalla FC, Abeliovich H, Abraham RT, Acevedo-Arozena A, Adeli K, Agholme L, Agnello M, Agostinis P, Aguirre-Ghiso JA, et al. Guidelines for the use and interpretation of assays for monitoring autophagy. Autophagy 2012; 8:445-544; PMID:22966490; http://dx.doi.org/10.4161/auto.19496
27 Liang C, Feng P, Ku B, Dotan I, Canaani D, Oh BH, Jung JU. Autophagic and tumour suppressor activity of a novel Beclin1-binding protein UVRAG. Nat Cell Biol 2006; 8:688-99; PMID:16799551; http://dx.doi.org/10.1038/ncb1426
28 Liang C, Lee JS, Inn KS, Gack MU, Li Q, Roberts EA, Vergne I, Deretic V, Feng P, Akazawa C, et al. Beclin1-binding UVRAG targets the class C Vps complex to coordinate autophagosome maturation and endocytic trafficking. Nat Cell Biol 2008; 10:776-87; PMID:18552835; http://dx.doi.org/10.1038/ncb1740
29 Itakura E, Kishi C, Inoue K, Mizushima N. Beclin 1 forms two distinct phosphatidylinositol 3-kinase complexes with mammalian Atg14 and UVRAG. Mol Biol Cell 2008; 19:5360-72; PMID:18843052; http://dx.doi.org/10.1091/mbc.E08-01-0080
30 Bekri S, Adelaide J, Merscher S, Grosgeorge J, Caroli-Bosc F, Perucca-Lostanlen D, Kelley PM, Pébusque MJ, Theillet C, Birnbaum D, et al. Detailed map of a region commonly amplified at 11q13–>q14 in human breast carcinoma. Cytogenet Cell Genet 1997; 79:125-31; PMID:9533029; http://dx.doi.org/10.1159/000134699
31 Yin X, Cao L, Kang R, Yang M, Wang Z, Peng Y, Tan Y, Liu L, Xie M, Zhao Y, et al. UV irradiation resistance-associated gene suppresses apoptosis by interfering with BAX activation. EMBO Rep 2011; 12:727-34; PMID:21597469; http://dx.doi.org/10.1038/embor.2011.79
32 Zhao Z, Oh S, Li D, Ni D, Pirooz SD, Lee JH, Yang S, Lee JY, Ghozalli I, Costanzo V, et al. A dual role for UVRAG in maintaining chromosomal stability independent of autophagy. Dev Cell 2012; 22:1001-16; PMID:22542840; http://dx.doi.org/10.1016/j.devcel.2011.12.027
33 Lee Y, Ahn C, Han J, Choi H, Kim J, Yim J, Lee J, Provost P, Rådmark O, Kim S, et al. The nuclear RNase III Drosha initiates microRNA processing. Nature 2003; 425:415-9; PMID:14508493; http://dx.doi.org/10.1038/nature01957
34 Kim KY, Hwang YJ, Jung MK, Choe J, Kim Y, Kim S, Lee CJ, Ahn H, Lee J, Kowall NW, et al. A multifunctional protein EWS regulates the expression of Drosha and microRNAs. Cell Death Differ 2014; 21(1):136-45; PMID:24185621; http://dx.doi.org/10.1038/cdd.2013.144
35 Kim SW, Ramasamy K, Bouamar H, Lin AP, Jiang D, Aguiar RC. MicroRNAs miR-125a and miR-125b constitutively activate the NF-kappaB pathway by targeting the tumor necrosis factor alpha-induced protein 3 (TNFAIP3, A20). Proc Natl Acad Sci U S A 2012; 109:7865-70; PMID:22550173; http://dx.doi.org/10.1073/pnas.1200081109
36 Muddashetty RS, Nalavadi VC, Gross C, Yao X, Xing L, Laur O, Warren ST, Bassell GJ. Reversible inhibition of PSD-95 mRNA translation by miR-125a, FMRP phosphorylation, and mGluR signaling. Mol Cell 2011; 42:673-88; PMID:21658607; http://dx.doi.org/10.1016/j.molcel.2011.05.006
37 Guo S, Lu J, Schlanger R, Zhang H, Wang JY, Fox MC, Purton LE, Fleming HH, Cobb B, Merkenschlager M, et al. MicroRNA miR-125a controls hematopoietic stem cell number. Proc Natl Acad Sci U S A 2010; 107:14229-34; PMID:20616003; http://dx.doi.org/10.1073/pnas.0913574107
38 Zhang Y, Gao JS, Tang X, Tucker LD, Quesenberry P, Rigoutsos I, Ramratnam B. MicroRNA 125a and its regulation of the p53 tumor suppressor gene. FEBS Lett 2009; 583:3725-30; PMID:19818772; http://dx.doi.org/10.1016/j.febslet.2009.10.002
39 Li X, Feng R, Huang C, Wang H, Wang J, Zhang Z, Yan H, Wen T. MicroRNA-351 regulates TMEM 59 (DCF1) expression and mediates neural stem cell morphogenesis. RNA Biol 2012; 9(3):292-301; PMID:22336716; http://dx.doi.org/10.4161/rna.19100
40 Chen Y, Melton DW, Gelfond JA, McManus LM, Shireman PK. MiR-351 transiently increases during muscle regeneration and promotes progenitor cell proliferation and survival upon differentiation. Physiol Genomics 2012; 44:1042-51; PMID:22968638; http://dx.doi.org/10.1152/physiolgenomics.00052.2012
41 Wang Y, Jiang XL, Yang SC, Lin X, He Y, Yan C, Wu L, Chen GQ, Wang ZY, Wu Q. MicroRNAs in the regulation of interfacial behaviors of MSCs cultured on microgrooved surface pattern. Biomaterials 2011; 32:9207-17; PMID:21890196; http://dx.doi.org/10.1016/j.biomaterials.2011.08.058
42 Funderburk SF, Wang QJ, Yue Z. The Beclin 1-VPS34 complex–at the crossroads of autophagy and beyond. Trends Cell Biol 2010; 20:355-62; PMID:20356743; http://dx.doi.org/10.1016/j.tcb.2010.03.002
43 Jiang P, Nishimura T, Sakamaki Y, Itakura E, Hatta T, Natsume T, Mizushima N. Mizushima N. The HOPS complex mediates autophagosome-lysosome fusion through interaction with syntaxin 17. Mol Biol Cell 2014; 25(8):1327-37; PMID:24554770; http://dx.doi.org/10.1091/mbc.E13-08-0447
44 Takáts S, Pircs K, Nagy P, Varga Á, Kárpáti M, Hegedűs K, Kramer H, Kovács AL, Sass M, Juhász G. Interaction of the HOPS complex with Syntaxin 17 mediates autophagosome clearance in Drosophila. Mol Biol Cell 2014; 25(8):1338-54; PMID:24554766; http://dx.doi.org/10.1091/mbc.E13-08-0449
45 Knævelsrud H, Ahlquist T, Merok MA, Nesbakken A, Stenmark H, Lothe RA, Simonsen A. UVRAG mutations associated with microsatellite unstable colon cancer do not affect autophagy. Autophagy 2010; 6(7):863-70; PMID:20724836; http://dx.doi.org/10.4161/auto.6.7.13033
46 Sun Q, Fan W, Chen K, Ding X, Chen S, Zhong Q. Identification of Barkor as a mammalian autophagy-specific factor for Beclin 1 and class III phosphatidylinositol 3-kinase. Proc Natl Acad Sci U S A 2008; 105:19211-6; PMID:19050071; http://dx.doi.org/10.1073/pnas.0810452105
47 Høyer-Hansen M, Bastholm L, Mathiasen IS, Elling F, Jäättelä M. Vitamin D analog EB1089 triggers dramatic lysosomal changes and Beclin 1-mediated autophagic cell death. Cell Death Differ 2005; 12(10):1297-309; PMID:15905882
48 Wu TD, Nacu S. Fast and SNP-tolerant detection of complex variants and splicing in short reads. Bioinformatics 2010; 26:873-81; PMID:20147302; http://dx.doi.org/10.1093/bioinformatics/btq057
49 Mortazavi A, Williams BA, McCue K, Schaeffer L, Wold B. Mapping and quantifying mammalian transcriptomes by RNA-Seq. Nat Methods 2008; 5:621-8; PMID:18516045; http://dx.doi.org/10.1038/nmeth.1226
50 Smoot ME, Ono K, Ruscheinski J, Wang PL, Ideker T. Cytoscape 2.8: new features for data integration and network visualization. Bioinformatics 2011; 27:431-2; PMID:21149340; http://dx.doi.org/10.1093/bioinformatics/btq675